Radiation efficiency and surface waves for patch antennas on inhomogeneous substrat

Kristensson, Gerhard; Abdelmassih Waller, Peter; Derneryd, Anders

2001

CODEN:LUTEDX/(TEAT-7100)/1-48/(2001)

Revision No. 1: May 2002

Radiation efficiency and surface waves for patch antennas on inhomogeneous substrates

Gerhard Kristensson, Peter Waller, and Anders Derneryd

Department of Electroscience
Electromagnetic Theory
Lund Institute of Technology
Sweden

Gerhard Kristensson (Gerhard.Kristensson@es.lth.se)
Peter Waller (Peter.Waller@es.lth.se)
Anders Derneryd (Anders.Derneryd@es.lth.se)

Department of Electroscience
Electromagnetic Theory
Lund Institute of Technology
P.O. Box 118
SE-221 00 Lund
Sweden

Editor: Gerhard Kristensson

Abstract

In this paper the surface wave characteristics, as well as the radiation efficiency and the directivity of a patch antenna, with a given current distribution, located on top of an inhomogeneous, isotropic substrate are calculated. The substrate is infinite in the lateral directions and inhomogeneous with respect to the height coordinate. The surface waves in the substrate are analyzed using the propagator technique and residue calculus. The propagators and the residues are found by solving two sets of systems of ordinary differential equations (ODEs). Several dispersion curves of the surface waves for inhomogeneous substrates are calculated. The radiation efficiency and the directivity are compared with the corresponding quantities of a printed antenna on a homogenized substrate. Moreover, some alternative ways of calculating the reflection dyadic of an inhomogeneous substrate are presented in a series of appendices.

1 Introduction

The radiation efficiency and directivity of printed antennas have been of current interest during recent decades, see *e.g.*, [2, 14, 16, 20, 25, 39]. One reason for this interest is the widely use of microstrip patch antennas in communication systems, as well as their low profile and low weight.

Several ways of increasing the radiation efficiency of the printed antenna, and to suppress radiation in the lateral directions, have been proposed. Vegni *et al.* report that certain inhomogeneous profiles show improved directivity and bandwidth, as well as improved matching characteristics [39]. A superstrate can also increase the performance of the antenna [37, 38].

The power transferred into the surface wave modes does not contribute to the main radiation, but is scattered off the edges of the finite ground plane and gives rise to spurious radiation. In this paper a characterization of surface waves in grounded, inhomogeneous, infinite dielectric slabs is addressed. Moreover, we investigate the role of an inhomogeneous substrate to suppress the surface waves and to increase the radiation efficiency of the antenna.

Wave propagation in inhomogeneous materials is clearly presented in many textbooks, see *e.g.*, [6, 9, 41]. An investigation of inhomogeneous patch antenna substrates is found in *e.g.*, [5, 26–28, 39, 40]. Analysis of surface waves in patch antenna substrates is, for an example, found in [2, 13, 16, 19, 20, 31].

The basic tool in the analysis in this paper is the notion of propagators. These propagators are thoroughly investigated in [34, 35]. The method has certain similarities with a vector generalization of the transmission line theory [12, 15, 32]. Specifically, the propagator technique is a vector generalization of the voltage-current transmission theory formulation [12] or transmission (ABCD) matrix [32]. In this paper, we prove that the concept of propagators is invaluable in the analysis of surface waves in inhomogeneous profiles, and that it provides a powerful tool for the analysis of all kinds of wave phenomena in an inhomogeneous substrate.

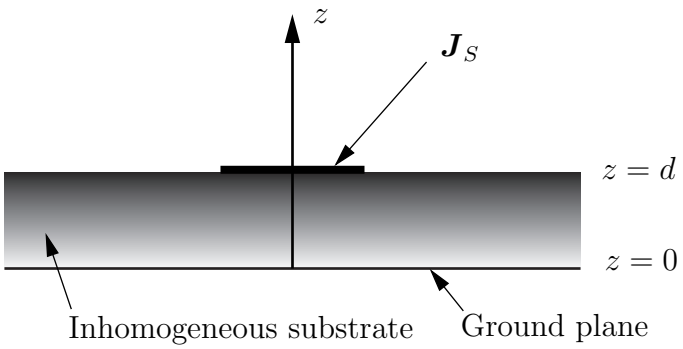

Figure 1: The geometry of the problem.

Firstly, we make pertinent representations of the fields inside and outside the substrate in terms of a lateral Fourier transform, and we state the fundamental equations these fields have to satisfy in the spectral domain. Moreover, the concept of propagators is presented, and we introduce the wave splitting concept for the fields outside the substrate to correctly cope with the radiation conditions in the upper half space. This is all done in Section 2. The solution to the radiation problem with propagators is presented in Section 3. The surface waves are characterized by the singular behavior of the propagator operator and these waves are analyzed in Section 4. Several dispersion curves of the surface waves are given for a series of pertinent permittivity profiles. The power radiated by the space and the surface waves are analyzed in Sections 5 and 6, respectively. The radiation efficiency and directivity are illustrated in a series of computations for different permittivity profiles. The paper ends with a series of appendices containing technical calculations and several efficient ways of computing the reflection dyadic or its inverse.

2 Theory

The geometry treated in this paper is depicted in Figure 1. The direction normal to the ground plane is denoted z. Let the ground plane be located at $z = 0$ and let the substrate fill up the space between $z = 0$ and $z = d$. The substrate is assumed to be an isotropic material characterized by the relative permittivity $\epsilon(z)$ and the relative permeability $\mu(z)$, which both can be inhomogeneous w.r.t. the depth coordinate z. The permittivity and permeability of vacuum are denoted by ϵ_0 and μ_0, respectively. At $z = d$ a finite patch (or several patches) of arbitrary shape is located. The surface current density on the patch is denoted $\boldsymbol{J}_S$, see Figure 1. In the half space above the patch, $z > d$, we assume vacuous conditions. The time convention adopted in this paper is $\exp(-\mathrm{i}\omega t)$.

In a laterally homogeneous geometry it is natural to decompose the fields in a spectrum of plane waves. The spatial Fourier transform of a time-harmonic field

$\boldsymbol{E}(\boldsymbol{r})$ with respect to the lateral vector variable $\boldsymbol{\rho} = \hat{\boldsymbol{x}}x + \hat{\boldsymbol{y}}y$ is defined by

$$\boldsymbol{E}(\boldsymbol{k}_t, z) = \iint_{-\infty}^{\infty} \boldsymbol{E}(\boldsymbol{r}) e^{-\mathrm{i}\boldsymbol{k}_t \cdot \boldsymbol{\rho}} \, \mathrm{d}x \, \mathrm{d}y \tag{2.1}$$

where

$$\boldsymbol{k}_t = \hat{\boldsymbol{x}}k_x + \hat{\boldsymbol{y}}k_y$$

is the lateral wave vector and the non-negative number

$$k_t = \sqrt{k_x^2 + k_y^2} \geq 0$$

is the lateral wave number. By the Fourier inversion formula, the inverse Fourier transform w.r.t. $\boldsymbol{\rho}$ is

$$\boldsymbol{E}(\boldsymbol{r}) = \frac{1}{4\pi^2} \iint_{-\infty}^{\infty} \boldsymbol{E}(\boldsymbol{k}_t, z) e^{\mathrm{i}\boldsymbol{k}_t \cdot \boldsymbol{\rho}} \, \mathrm{d}k_x \, \mathrm{d}k_y \tag{2.2}$$

Notice that, in order to avoid cumbersome notation, the same letter has been used to denote the Fourier transform of the field, $\boldsymbol{E}(\boldsymbol{k}_t, z)$, and the field itself, $\boldsymbol{E}(\boldsymbol{r})$, in real space. The argument of the field shows what field is intended.

The Fourier variable $\boldsymbol{k}_t$ defines two unit vectors in the x-y-plane, which constitutes the natural, coordinate-free basis for decomposing vectors and dyadics in the x-y-plane, *viz.*,

$$\hat{\boldsymbol{e}}_{\parallel} = \frac{\boldsymbol{k}_t}{k_t}, \qquad \hat{\boldsymbol{e}}_{\perp} = \mathbf{J} \cdot \hat{\boldsymbol{e}}_{\parallel}$$

where[1] $\mathbf{J} = \hat{\boldsymbol{z}} \times \mathbf{I}_3$ or $\mathbf{J} \cdot \boldsymbol{A} = \hat{\boldsymbol{z}} \times \boldsymbol{A}$, which denotes a projection of a vector $\boldsymbol{A}$ onto the x-y-plane followed by a rotation of $\pi/2$ in this plane. Notice that $\mathbf{J} \cdot \mathbf{J} = -\mathbf{I}_2$. Moreover, the normal (longitudinal) wave number, k_z, is defined by

$$k_z = \left(k_0^2 - k_t^2\right)^{1/2} = \begin{cases} \sqrt{k_0^2 - k_t^2} \text{ for } k_t < k_0 \\ \mathrm{i}\sqrt{k_t^2 - k_0^2} \text{ for } k_t > k_0 \end{cases} \tag{2.3}$$

where the wave number of vacuum is $k_0 = \omega\sqrt{\epsilon_0 \mu_0}$, and where the standard convention of the square root of a positive argument is intended.

All vector fields are decomposed into their transverse x-y-components and their z-components, *e.g.*,

$$\begin{cases} \boldsymbol{E}(\boldsymbol{r}) = \boldsymbol{E}_{xy}(\boldsymbol{r}) + \hat{\boldsymbol{z}} E_z(\boldsymbol{r}) \\ \boldsymbol{E}(\boldsymbol{k}_t, z) = \boldsymbol{E}_{xy}(\boldsymbol{k}_t, z) + \hat{\boldsymbol{z}} E_z(\boldsymbol{k}_t, z) \end{cases}$$

[1]Note the typographical difference between the dyadic $\mathbf{J}$ which denotes a rotation, and the current density vector $\boldsymbol{J}$. All vectors in this paper are typed in italic bold face and dyadics are typed in roman bold face. The identity dyadic in n dimensions is denoted $\mathbf{I}_n$.

2.1 The fundamental equation

A two-dimensional spatial Fourier transform (in the x-y plane) of the Maxwell equations transforms these equations into a set of first order ordinary differential equations (ODEs). This is possible since our material does not vary with x and y. If we solve for the transverse components, $\boldsymbol{E}_{xy}(\boldsymbol{k}_t, z)$ and $\boldsymbol{H}_{xy}(\boldsymbol{k}_t, z)$, we get the fundamental equation, *i.e.*, the transverse component of the fields satisfy

$$\begin{aligned}\frac{\mathrm{d}}{\mathrm{d}z}\begin{pmatrix}\boldsymbol{E}_{xy}(\boldsymbol{k}_t,z)\\ \eta_0\mathbf{J}\cdot\boldsymbol{H}_{xy}(\boldsymbol{k}_t,z)\end{pmatrix} =&\mathrm{i}k_0\begin{pmatrix}\mathbf{M}_{11}(\boldsymbol{k}_t,z) & \mathbf{M}_{12}(\boldsymbol{k}_t,z)\\ \mathbf{M}_{21}(\boldsymbol{k}_t,z) & \mathbf{M}_{22}(\boldsymbol{k}_t,z)\end{pmatrix}\cdot\begin{pmatrix}\boldsymbol{E}_{xy}(\boldsymbol{k}_t,z)\\ \eta_0\mathbf{J}\cdot\boldsymbol{H}_{xy}(\boldsymbol{k}_t,z)\end{pmatrix}\\ &+\eta_0\begin{pmatrix}\boldsymbol{k}_t J_z(\boldsymbol{k}_t,z)/\left(k_0\epsilon(z)\right)\\ \boldsymbol{J}_{xy}(\boldsymbol{k}_t,z)\end{pmatrix}\\ =\mathrm{i}k_0\mathbf{M}(\boldsymbol{k}_t,z)\cdot&\begin{pmatrix}\boldsymbol{E}_{xy}(\boldsymbol{k}_t,z)\\ \eta_0\mathbf{J}\cdot\boldsymbol{H}_{xy}(\boldsymbol{k}_t,z)\end{pmatrix}+\eta_0\begin{pmatrix}\boldsymbol{k}_t J_z(\boldsymbol{k}_t,z)/\left(k_0\epsilon(z)\right)\\ \boldsymbol{J}_{xy}(\boldsymbol{k}_t,z)\end{pmatrix}\end{aligned} \tag{2.4}$$

The 2×2 dyadics $\mathbf{M}_{ij}$, $i,j=1,2$, can readily be found, see [35]. For an isotropic material, these dyadics are explicitly given by, see (A.5) and the short derivation in Appendix A

$$\begin{cases}\mathbf{M}_{11}(\boldsymbol{k}_t,z)=\mathbf{M}_{22}(\boldsymbol{k}_t,z)=\mathbf{0}\\ \mathbf{M}_{12}(\boldsymbol{k}_t,z)=\dfrac{\boldsymbol{k}_t\boldsymbol{k}_t}{k_0^2\epsilon(z)}-\mu(z)\mathbf{I}_2=\left(\dfrac{k_t^2}{k_0^2\epsilon(z)}-\mu(z)\right)\hat{\boldsymbol{e}}_{\parallel}\hat{\boldsymbol{e}}_{\parallel}-\mu(z)\hat{\boldsymbol{e}}_{\perp}\hat{\boldsymbol{e}}_{\perp}\\ \mathbf{M}_{21}(\boldsymbol{k}_t,z)=-\dfrac{\mathbf{J}\cdot\boldsymbol{k}_t\boldsymbol{k}_t\cdot\mathbf{J}}{k_0^2\mu(z)}-\epsilon(z)\mathbf{I}_2=\left(\dfrac{k_t^2}{k_0^2\mu(z)}-\epsilon(z)\right)\hat{\boldsymbol{e}}_{\perp}\hat{\boldsymbol{e}}_{\perp}-\epsilon(z)\hat{\boldsymbol{e}}_{\parallel}\hat{\boldsymbol{e}}_{\parallel}\end{cases} \tag{2.5}$$

In these expressions the transverse current density, $\boldsymbol{J}_{xy}$, is related to the surface current density, $\boldsymbol{J}_S$, as $\boldsymbol{J}_S=\delta(z-d)\boldsymbol{J}_{xy}$.

From the knowledge of the tangential fields, $\boldsymbol{E}_{xy}(\boldsymbol{k}_t,z)$ and $\boldsymbol{H}_{xy}(\boldsymbol{k}_t,z)$, we obtain the z-components. In the absence of J_z, we get, see (A.6)

$$\begin{cases}E_z(\boldsymbol{k}_t,z)=\dfrac{\eta_0}{k_0\epsilon(z)}\boldsymbol{k}_t\cdot\mathbf{J}\cdot\boldsymbol{H}_{xy}(\boldsymbol{k}_t,z)\\ \eta_0 H_z(\boldsymbol{k}_t,z)=-\dfrac{1}{k_0\mu(z)}\boldsymbol{k}_t\cdot\mathbf{J}\cdot\boldsymbol{E}_{xy}(\boldsymbol{k}_t,z)\end{cases} \tag{2.6}$$

The generalization of the dynamics in (2.4) to general linear materials (bianisotropic materials) is found in [35].

2.2 Propagators

In this section, we introduce the concept of propagators of fields. A more thorough treatment of these propagators is found in [23, 34, 35]. The propagators relates the total transverse fields at two different z-values to each other, and therefore they constitute the mapping of the transverse field at one position, $z=z_1$, to the transverse fields at another position, $z=z_2$, see Figure 2. The explicit representation of the propagators are easily found in the Fourier transform (spectral) domain. The

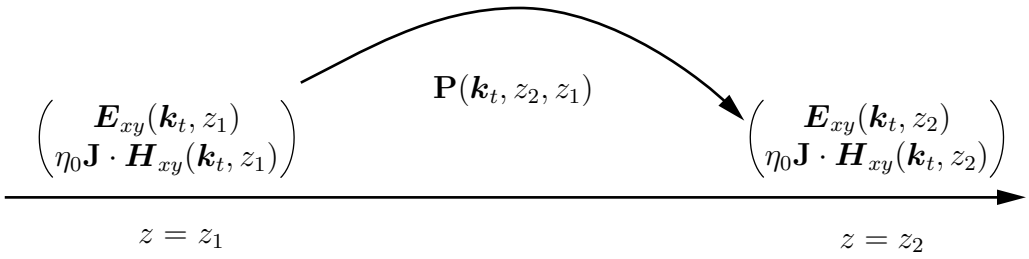

Figure 2: The propagator dyadic, $\mathbf{P}(\boldsymbol{k}_t, z_2, z_1)$, that relates the transverse fields at $z = z_1$ and z_2 to each other.

explicit expressions of the propagator dyadics $\mathbf{P}_{ij}$, $i, j = 1, 2$, which relate the total transverse fields at $z = z_1$ and z_2 to each other, are

$$\begin{aligned} \begin{pmatrix} \boldsymbol{E}_{xy}(\boldsymbol{k}_t, z_2) \\ \eta_0 \mathbf{J} \cdot \boldsymbol{H}_{xy}(\boldsymbol{k}_t, z_2) \end{pmatrix} &= \mathbf{P}(\boldsymbol{k}_t, z_2, z_1) \cdot \begin{pmatrix} \boldsymbol{E}_{xy}(\boldsymbol{k}_t, z_1) \\ \eta_0 \mathbf{J} \cdot \boldsymbol{H}_{xy}(\boldsymbol{k}_t, z_1) \end{pmatrix} \\ &= \begin{pmatrix} \mathbf{P}_{11}(\boldsymbol{k}_t, z_2, z_1) & \mathbf{P}_{12}(\boldsymbol{k}_t, z_2, z_1) \\ \mathbf{P}_{21}(\boldsymbol{k}_t, z_2, z_1) & \mathbf{P}_{22}(\boldsymbol{k}_t, z_2, z_1) \end{pmatrix} \cdot \begin{pmatrix} \boldsymbol{E}_{xy}(\boldsymbol{k}_t, z_1) \\ \eta_0 \mathbf{J} \cdot \boldsymbol{H}_{xy}(\boldsymbol{k}_t, z_1) \end{pmatrix} \end{aligned} \tag{2.7}$$

This formulation is a vector generalization of the voltage-current transmission theory formulation [12] or transmission (ABCD) matrix [32]. The dyadic $\mathbf{P}(\boldsymbol{k}_t, z_2, z_1)$ has, in general, 16 non-zero components, and transforms the fields from an initial position at $z = z_1$ to the final position at $z = z_2$. The order of the z-arguments in the propagator is therefore important.

The four two-dimensional propagator dyadics, $\mathbf{P}_{ij}$, $i, j = 1, 2$, satisfy the same set of ordinary differential equations (ODE) as the fields [35], see (2.4), *i.e.*,

$$\frac{\mathrm{d}}{\mathrm{d}z}\mathbf{P}(\boldsymbol{k}_t, z, z_1) = \mathrm{i}k_0 \mathbf{M}(\boldsymbol{k}_t, z) \cdot \mathbf{P}(\boldsymbol{k}_t, z, z_1) \tag{2.8}$$

together with the initial condition

$$\mathbf{P}(\boldsymbol{k}_t, z_1, z_1) = \begin{pmatrix} \mathbf{P}_{11}(\boldsymbol{k}_t, z_1, z_1) & \mathbf{P}_{12}(\boldsymbol{k}_t, z_1, z_1) \\ \mathbf{P}_{21}(\boldsymbol{k}_t, z_1, z_1) & \mathbf{P}_{22}(\boldsymbol{k}_t, z_1, z_1) \end{pmatrix} = \begin{pmatrix} \mathbf{I}_2 & \mathbf{0} \\ \mathbf{0} & \mathbf{I}_2 \end{pmatrix} = \mathbf{I}_4$$

This set of ordinary equations is, in general, a relation between the 16 components of the propagator $\mathbf{P}(\boldsymbol{k}_t, z, z_1)$. The propagators are dimensionless quantities.

Note that the propagator $\mathbf{P}(\boldsymbol{k}_t, z_1, z_1)$ is an analytic dyadic in the parameter $\boldsymbol{k}_t$ since $\mathbf{M}(\boldsymbol{k}_t, z)$ and the initial conditions are analytic in the parameter $\boldsymbol{k}_t$ [18, 43]. This important conclusion is used later in this paper.

In a vacuous region, *e.g.*, $z > d$, the explicit form of the propagators are easy to find. The result is [35]

$$\mathbf{P}(\boldsymbol{k}_t, z, z_1) = \mathbf{I}_4 \cos\left[k_z(z - z_1)\right] + \frac{ik_0}{k_z}\mathbf{M}_0(\boldsymbol{k}_t) \sin\left[k_z(z - z_1)\right]$$

where k_z is defined in (2.3) and

$$\mathbf{M}_0(\boldsymbol{k}_t) = \begin{pmatrix} \mathbf{0} & -\frac{k_z^2}{k_0^2}\hat{\boldsymbol{e}}_\parallel\hat{\boldsymbol{e}}_\parallel - \hat{\boldsymbol{e}}_\perp\hat{\boldsymbol{e}}_\perp \\ -\frac{k_z^2}{k_0^2}\hat{\boldsymbol{e}}_\perp\hat{\boldsymbol{e}}_\perp - \hat{\boldsymbol{e}}_\parallel\hat{\boldsymbol{e}}_\parallel & \mathbf{0} \end{pmatrix}$$

2.2.1 Inhomogeneous isotropic material

Since this paper only treats isotropic materials, we explicitly write down the expressions of the equation (2.8) above for this class of materials. The dynamics of the propagator in a source free isotropic material is (2.5)

$$\frac{\mathrm{d}}{\mathrm{d}z}\begin{pmatrix} \mathbf{P}_{11}(z,z_1) & \mathbf{P}_{12}(z,z_1) \\ \mathbf{P}_{21}(z,z_1) & \mathbf{P}_{22}(z,z_1) \end{pmatrix} = \mathrm{i}k_0 \begin{pmatrix} \mathbf{0} & \mathbf{M}_{12}(z) \\ \mathbf{M}_{21}(z) & \mathbf{0} \end{pmatrix} \cdot \begin{pmatrix} \mathbf{P}_{11}(z,z_1) & \mathbf{P}_{12}(z,z_1) \\ \mathbf{P}_{21}(z,z_1) & \mathbf{P}_{22}(z,z_1) \end{pmatrix}$$

where

$$\begin{cases} \mathbf{M}_{12}(z) = \left(\dfrac{k_t^2}{k_0^2\epsilon(z)} - \mu(z)\right)\hat{\boldsymbol{e}}_\parallel\hat{\boldsymbol{e}}_\parallel - \mu(z)\hat{\boldsymbol{e}}_\perp\hat{\boldsymbol{e}}_\perp \\ \mathbf{M}_{21}(z) = \left(\dfrac{k_t^2}{k_0^2\mu(z)} - \epsilon(z)\right)\hat{\boldsymbol{e}}_\perp\hat{\boldsymbol{e}}_\perp - \epsilon(z)\hat{\boldsymbol{e}}_\parallel\hat{\boldsymbol{e}}_\parallel \end{cases}$$

with initial condition

$$\begin{cases} \mathbf{P}_{11}(z_1,z_1) = \mathbf{P}_{22}(z_1,z_1) = \mathbf{I}_2 \\ \mathbf{P}_{21}(z_1,z_1) = \mathbf{P}_{12}(z_1,z_1) = \mathbf{0} \end{cases}$$

We immediately see that these equations split into two non-coupling sets, *viz.*,

$$\begin{cases} \dfrac{\mathrm{d}}{\mathrm{d}z}\mathbf{P}_{11}(z,z_1) = \mathrm{i}k_0\mathbf{M}_{12}(z)\cdot\mathbf{P}_{21}(z,z_1) \\ \dfrac{\mathrm{d}}{\mathrm{d}z}\mathbf{P}_{21}(z,z_1) = \mathrm{i}k_0\mathbf{M}_{21}(z)\cdot\mathbf{P}_{11}(z,z_1) \end{cases} \tag{2.9}$$

and

$$\begin{cases} \dfrac{\mathrm{d}}{\mathrm{d}z}\mathbf{P}_{12}(z,z_1) = \mathrm{i}k_0\mathbf{M}_{12}(z)\cdot\mathbf{P}_{22}(z,z_1) \\ \dfrac{\mathrm{d}}{\mathrm{d}z}\mathbf{P}_{22}(z,z_1) = \mathrm{i}k_0\mathbf{M}_{21}(z)\cdot\mathbf{P}_{12}(z,z_1) \end{cases} \tag{2.10}$$

which is a relation between two of the propagators $\mathbf{P}_{ij}(z,z_1)$.

An additional reduction of the coupling between the components of the propagators can be made in the isotropic case. In a $\{\parallel,\perp\}$-coordinate representation, we get the TM-case and the TE-case, respectively, which both lead to a set of ODEs between two scalar components of the propagators. We introduce the notation

$$\mathbf{P}_{ij} = \hat{\boldsymbol{e}}_\parallel\hat{\boldsymbol{e}}_\parallel P_{ij}^{\mathrm{TM}} + \hat{\boldsymbol{e}}_\perp\hat{\boldsymbol{e}}_\perp P_{ij}^{\mathrm{TE}}, \qquad i,j = 1,2$$

The TM-case, $\parallel$-polarization, splits in two non-coupling sets of first order ordinary differential equations

$$\begin{cases} \dfrac{\mathrm{d}}{\mathrm{d}z}P_{11}^{\mathrm{TM}} = \mathrm{i}k_0\left(\dfrac{k_t^2}{k_0^2\epsilon(z)} - \mu(z)\right)P_{21}^{\mathrm{TM}} \\ \dfrac{\mathrm{d}}{\mathrm{d}z}P_{21}^{\mathrm{TM}} = -\mathrm{i}k_0\epsilon(z)P_{11}^{\mathrm{TM}} \end{cases} \qquad \begin{cases} P_{11}^{\mathrm{TM}}(z_1,z_1) = 1 \\ P_{21}^{\mathrm{TM}}(z_1,z_1) = 0 \end{cases}$$

and

$$\begin{cases} \dfrac{\mathrm{d}}{\mathrm{d}z}P_{12}^{\mathrm{TM}} = \mathrm{i}k_0\left(\dfrac{k_t^2}{k_0^2\epsilon(z)} - \mu(z)\right)P_{22}^{\mathrm{TM}} \\ \dfrac{\mathrm{d}}{\mathrm{d}z}P_{22}^{\mathrm{TM}} = -\mathrm{i}k_0\epsilon(z)P_{12}^{\mathrm{TM}} \end{cases} \qquad \begin{cases} P_{12}^{\mathrm{TM}}(z_1,z_1) = 0 \\ P_{22}^{\mathrm{TM}}(z_1,z_1) = 1 \end{cases} \tag{2.11}$$

Note that the equations are similar, but the initial conditions differ.

For the other polarization, $\perp$-polarization, we obtain the TE-case, which also splits in two non-coupling sets of first order ordinary differential equations.

$$\begin{cases} \dfrac{\mathrm{d}}{\mathrm{d}z}P_{11}^{\mathrm{TE}} = -\mathrm{i}k_0\mu(z)P_{21}^{\mathrm{TE}} \\ \dfrac{\mathrm{d}}{\mathrm{d}z}P_{21}^{\mathrm{TE}} = \mathrm{i}k_0\left(\dfrac{k_t^2}{k_0^2\mu(z)} - \epsilon(z)\right)P_{11}^{\mathrm{TE}} \end{cases} \qquad \begin{cases} P_{11}^{\mathrm{TE}}(z_1,z_1) = 1 \\ P_{21}^{\mathrm{TE}}(z_1,z_1) = 0 \end{cases}$$

and

$$\begin{cases} \dfrac{\mathrm{d}}{\mathrm{d}z}P_{12}^{\mathrm{TE}} = -\mathrm{i}k_0\mu(z)P_{22}^{\mathrm{TE}} \\ \dfrac{\mathrm{d}}{\mathrm{d}z}P_{22}^{\mathrm{TE}} = \mathrm{i}k_0\left(\dfrac{k_t^2}{k_0^2\mu(z)} - \epsilon(z)\right)P_{12}^{\mathrm{TE}} \end{cases} \qquad \begin{cases} P_{12}^{\mathrm{TE}}(z_1,z_1) = 0 \\ P_{22}^{\mathrm{TE}}(z_1,z_1) = 1 \end{cases} \tag{2.12}$$

Again, the equations are similar, but the initial conditions differ.

An asymptotic analysis of the ODEs in (2.11) and (2.12) as $k_0 d \to 0$ gives the following result:

$$\begin{cases} P_{12}^{\mathrm{TM}}(\boldsymbol{k}_t, d, 0) = \mathrm{i}k_0 d\left(\dfrac{k_t^2}{k_0^2\epsilon_h} - \mu_h\right) + O\left((k_0 d)^3\right) \\ P_{22}^{\mathrm{TM}}(\boldsymbol{k}_t, d, 0) = 1 + O\left((k_0 d)^2\right) \end{cases}$$

and

$$\begin{cases} P_{12}^{\mathrm{TE}}(\boldsymbol{k}_t, d, 0) = -\mathrm{i}k_0 d\mu_h + O\left((k_0 d)^3\right) \\ P_{22}^{\mathrm{TE}}(\boldsymbol{k}_t, d, 0) = 1 + O\left((k_0 d)^2\right) \end{cases}$$

where the homogenized values of the relative permittivity, ϵ_h, and the relative permeability, μ_h, are [33]

$$\frac{d}{\epsilon_h} = \int_0^d \frac{1}{\epsilon(z)}\,\mathrm{d}z, \qquad \mu_h = \frac{1}{d}\int_0^d \mu(z)\,\mathrm{d}z \tag{2.13}$$

Note that all propagators for the isotropic case $P_{ij}^{\mathrm{TM,TE}}(z, z_1)$ are even functions in the parameter k_t, and that the propagators are analytic functions in the parameter $\boldsymbol{k}_t$ (only the modulus of $\boldsymbol{k}_t$ enters).

If the isotropic material is homogeneous, *i.e.*, $\epsilon(z) = \epsilon$ and $\mu(z) = \mu$, then the explicit solution of the propagators in a homogenous, isotropic material can be found. The result is [35]

$$\mathbf{P}(\boldsymbol{k}_t, z, z_1) = \mathbf{I}_4 \cos\left[k_0(z - z_1)\kappa\right] + \frac{i}{\kappa}\mathbf{M}(\boldsymbol{k}_t)\sin\left[k_0(z - z_1)\kappa\right] \tag{2.14}$$

where

$$\mathbf{M}(\boldsymbol{k}_t) = \begin{pmatrix} \mathbf{0} & -\mu\mathbf{I}_2 + \frac{1}{\epsilon k_0^2}\boldsymbol{k}_t\boldsymbol{k}_t \\ -\epsilon\mathbf{I}_2 - \frac{1}{\mu k_0^2}\mathbf{J}\cdot\boldsymbol{k}_t\boldsymbol{k}_t\cdot\mathbf{J} & \mathbf{0} \end{pmatrix}$$

and where

$$\kappa^2 = \epsilon\mu - k_t^2/k_0^2$$

2.3 Wave splitting

The correct radiation in the half space region $z > d$ has to be satisfied. In the geometry studied in this paper, only the field components that carry power in the positive z-direction are permitted. To guarantee this condition, we need to split the fields into two new fields—one transporting power in the positive z-direction and one in the negative z-direction. This wave splitting provides us with a systematic way of keeping the correct components of the field in the half space $z > d$. The splitting in vacuum is given by [35] (for additional references, see *e.g.*, [30] and for transient fields *e.g.*, [17])

$$\begin{pmatrix} \boldsymbol{F}^+(\boldsymbol{k}_t, z) \\ \boldsymbol{F}^-(\boldsymbol{k}_t, z) \end{pmatrix} = \frac{1}{2}\begin{pmatrix} \mathbf{I}_2 & -\mathbf{W}(\boldsymbol{k}_t) \\ \mathbf{I}_2 & \mathbf{W}(\boldsymbol{k}_t) \end{pmatrix}\cdot\begin{pmatrix} \boldsymbol{E}_{xy}(\boldsymbol{k}_t, z) \\ \eta_0\mathbf{J}\cdot\boldsymbol{H}_{xy}(\boldsymbol{k}_t, z) \end{pmatrix} \tag{2.15}$$

The splitting dyadic $\mathbf{W}$ and its inverse $\mathbf{W}^{-1}$ are defined by

$$\begin{cases} \mathbf{W}(\boldsymbol{k}_t) = \dfrac{k_z}{k_0}\left(\mathbf{I}_2 - \dfrac{1}{k_z^2}\boldsymbol{k}_t\times(\boldsymbol{k}_t\times\mathbf{I}_2)\right) = \dfrac{k_z}{k_0}\hat{\boldsymbol{e}}_\parallel\hat{\boldsymbol{e}}_\parallel + \dfrac{k_0}{k_z}\hat{\boldsymbol{e}}_\perp\hat{\boldsymbol{e}}_\perp \\ \mathbf{W}^{-1}(\boldsymbol{k}_t) = \dfrac{k_0}{k_z}\left(\mathbf{I}_2 + \dfrac{1}{k_0^2}\boldsymbol{k}_t\times(\boldsymbol{k}_t\times\mathbf{I}_2)\right) = \dfrac{k_0}{k_z}\hat{\boldsymbol{e}}_\parallel\hat{\boldsymbol{e}}_\parallel + \dfrac{k_z}{k_0}\hat{\boldsymbol{e}}_\perp\hat{\boldsymbol{e}}_\perp \end{cases} \tag{2.16}$$

Note the similarity between the splitting dyadic $\mathbf{W}$ and the admittance dyadic $\mathbf{Y}(\boldsymbol{k}_t)$ given by

$$\mathbf{Y}(\boldsymbol{k}_t) = \frac{1}{k_0 k_z}\left\{k_0^2\hat{\boldsymbol{e}}_\perp\hat{\boldsymbol{e}}_\parallel - k_z^2\hat{\boldsymbol{e}}_\parallel\hat{\boldsymbol{e}}_\perp\right\} = \mathbf{J}\cdot\mathbf{W}^{-1}(\boldsymbol{k}_t)$$

The field $\boldsymbol{F}^+$ ($\boldsymbol{F}^-$) transports power in the +(-)z-direction [21, 35], and, in general, the transverse electric field is the sum of the two split fields, *i.e.*,

$$\boldsymbol{E}_{xy}(\boldsymbol{k}_t, z) = \boldsymbol{F}^+(\boldsymbol{k}_t, z) + \boldsymbol{F}^-(\boldsymbol{k}_t, z)$$

The inverse of the wave splitting transformation, (2.15), is

$$\begin{pmatrix} \boldsymbol{E}_{xy}(\boldsymbol{k}_t, z) \\ \eta_0\mathbf{J}\cdot\boldsymbol{H}_{xy}(\boldsymbol{k}_t, z) \end{pmatrix} = \begin{pmatrix} \mathbf{I}_2 & \mathbf{I}_2 \\ -\mathbf{W}^{-1}(\boldsymbol{k}_t) & \mathbf{W}^{-1}(\boldsymbol{k}_t) \end{pmatrix}\cdot\begin{pmatrix} \boldsymbol{F}^+(\boldsymbol{k}_t, z) \\ \boldsymbol{F}^-(\boldsymbol{k}_t, z) \end{pmatrix} \tag{2.17}$$

Details about this transformation are found in Appendix B, where the dynamics of the fields $\boldsymbol{F}^+$ and $\boldsymbol{F}^-$ is derived. The result is, see (B.1)

$$\begin{aligned} \frac{\mathrm{d}}{\mathrm{d}z}\begin{pmatrix} \boldsymbol{F}^+(z) \\ \boldsymbol{F}^-(z) \end{pmatrix} =& \frac{\mathrm{i}k_0}{2}\begin{pmatrix} \mathbf{U}_{11}(z) & \mathbf{U}_{12}(z) \\ \mathbf{U}_{21}(z) & \mathbf{U}_{22}(z) \end{pmatrix}\cdot\begin{pmatrix} \boldsymbol{F}^+(z) \\ \boldsymbol{F}^-(z) \end{pmatrix} \\ &+ \frac{\eta_0}{2}\begin{pmatrix} \boldsymbol{k}_t J_z(z)/\left(k_0\epsilon(z)\right) - \mathbf{W}\cdot\boldsymbol{J}_{xy}(z) \\ \boldsymbol{k}_t J_z(z)/\left(k_0\epsilon(z)\right) + \mathbf{W}\cdot\boldsymbol{J}_{xy}(z) \end{pmatrix} \end{aligned} \tag{2.18}$$

where

$$\begin{pmatrix} \mathbf{U}_{11} & \mathbf{U}_{12} \\ \mathbf{U}_{21} & \mathbf{U}_{22} \end{pmatrix} = \begin{pmatrix} -\mathbf{W}\cdot\mathbf{M}_{21} - \mathbf{M}_{12}\cdot\mathbf{W}^{-1} & -\mathbf{W}\cdot\mathbf{M}_{21} + \mathbf{M}_{12}\cdot\mathbf{W}^{-1} \\ \mathbf{W}\cdot\mathbf{M}_{21} - \mathbf{M}_{12}\cdot\mathbf{W}^{-1} & \mathbf{W}\cdot\mathbf{M}_{21} + \mathbf{M}_{12}\cdot\mathbf{W}^{-1} \end{pmatrix} \tag{2.19}$$

In vacuum and no sources the dynamics simplifies to, see (B.8)

$$\frac{\mathrm{d}}{\mathrm{d}z}\begin{pmatrix} \boldsymbol{F}^+ \\ \boldsymbol{F}^- \end{pmatrix} = \mathrm{i}\begin{pmatrix} k_z\mathbf{I}_2 & \mathbf{0} \\ \mathbf{0} & -k_z\mathbf{I}_2 \end{pmatrix}\cdot\begin{pmatrix} \boldsymbol{F}^+ \\ \boldsymbol{F}^- \end{pmatrix}$$

From this expression, we conclude that the split fields decouple in vacuum and that the explicit solution in the half space $z > d$ is

$$\boldsymbol{F}^{\pm}(\boldsymbol{k}_t, z) = \boldsymbol{F}^{\pm}(\boldsymbol{k}_t, d^+)e^{\pm ik_z(z-d)} \tag{2.20}$$

3 Solution to the radiation problem

In this section, we solve the field above and in the grounded substrate, induced by a given surface current density, $\boldsymbol{J}_S$ by the use of the propagator technique. A more general treatment of this technique applied to bianisotropic materials is found in [23, 35]. Below, we simplify to the specific geometry adopted in this paper.

The propagator dyadics $\mathbf{P}_{ij}(\boldsymbol{k}_t, z, 0)$, $i, j = 1, 2$ relates the total fields at $z = 0$ and z, see (2.7). Specifically, inside the substrate we have

$$\begin{aligned}\begin{pmatrix} \boldsymbol{E}_{xy}(z) \\ \eta_0\mathbf{J}\cdot\boldsymbol{H}_{xy}(z) \end{pmatrix} &= \mathbf{P}(z,0)\cdot\begin{pmatrix} \boldsymbol{E}_{xy}(0) \\ \eta_0\mathbf{J}\cdot\boldsymbol{H}_{xy}(0) \end{pmatrix} \\ &= \begin{pmatrix} \mathbf{P}_{11}(z,0) & \mathbf{P}_{12}(z,0) \\ \mathbf{P}_{21}(z,0) & \mathbf{P}_{22}(z,0) \end{pmatrix}\cdot\begin{pmatrix} \boldsymbol{E}_{xy}(0) \\ \eta_0\mathbf{J}\cdot\boldsymbol{H}_{xy}(0) \end{pmatrix}, \qquad 0 \le z < d\end{aligned}$$

The boundary condition at $z = 0$, $\boldsymbol{E}_{xy}(0) = \mathbf{0}$, implies

$$\begin{pmatrix} \boldsymbol{E}_{xy}(z) \\ \eta_0\mathbf{J}\cdot\boldsymbol{H}_{xy}(z) \end{pmatrix} = \begin{pmatrix} \mathbf{P}_{12}(z,0)\cdot\eta_0\mathbf{J}\cdot\boldsymbol{H}_{xy}(0) \\ \mathbf{P}_{22}(z,0)\cdot\eta_0\mathbf{J}\cdot\boldsymbol{H}_{xy}(0) \end{pmatrix}, \qquad 0 \le z < d \tag{3.1}$$

In the region above the patch, we have, due to radiation conditions, only a $\boldsymbol{F}^+$ wave, $\boldsymbol{F}^- = \mathbf{0}$. The wave splitting, introduced in Section 2.3, gives, see (2.17)

$$\begin{pmatrix} \boldsymbol{E}_{xy}(z) \\ \eta_0\mathbf{J}\cdot\boldsymbol{H}_{xy}(z) \end{pmatrix} = \begin{pmatrix} \boldsymbol{F}^+(z) \\ -\mathbf{W}^{-1}\cdot\boldsymbol{F}^+(z) \end{pmatrix}, \qquad z > d \tag{3.2}$$

The $\boldsymbol{F}^+$ wave in vacuum is, see (2.20)

$$\boldsymbol{E}_{xy}(z) = \boldsymbol{F}^+(z) = \mathrm{e}^{\mathrm{i}k_z(z-d)}\boldsymbol{F}^+(d^+), \qquad z > d$$

Evaluate the equations (3.1) and (3.2) above and below the patch, *i.e.*, at $z = d^{\pm}$, respectively, and subtract. With the use of the boundary conditions on the patch, the result is

$$\begin{pmatrix} \mathbf{0} \\ \eta_0\boldsymbol{J}_S \end{pmatrix} = \begin{pmatrix} \boldsymbol{F}^+(d^+) \\ -\mathbf{W}^{-1}\cdot\boldsymbol{F}^+(d^+) \end{pmatrix} - \begin{pmatrix} \mathbf{P}_{12}(d,0)\cdot\eta_0\mathbf{J}\cdot\boldsymbol{H}_{xy}(0) \\ \mathbf{P}_{22}(d,0)\cdot\eta_0\mathbf{J}\cdot\boldsymbol{H}_{xy}(0) \end{pmatrix}$$

where the total surface current density on the patch is

$$\boldsymbol{J}_S = \mathbf{J} \cdot \boldsymbol{H}_{xy}(d^+) - \mathbf{J} \cdot \boldsymbol{H}_{xy}(d^-)$$

We solve for the unknown $\mathbf{J} \cdot \boldsymbol{H}_{xy}(0)$ and $\boldsymbol{F}^+(d^+)$. The result is

$$\begin{cases} \boldsymbol{F}^+(d^+) = -\mathbf{P}_{12}(d,0) \cdot \left(\mathbf{P}_{22}(d,0) + \mathbf{W}^{-1} \cdot \mathbf{P}_{12}(d,0)\right)^{-1} \cdot \eta_0 \boldsymbol{J}_S \\ \eta_0 \mathbf{J} \cdot \boldsymbol{H}_{xy}(0) = -\left(\mathbf{P}_{22}(d,0) + \mathbf{W}^{-1} \cdot \mathbf{P}_{12}(d,0)\right)^{-1} \cdot \eta_0 \boldsymbol{J}_S \end{cases} \tag{3.3}$$

Finally, the transverse electric and magnetic fields in the region $0 \leq z < d$ are, see (3.1)

$$\boldsymbol{E}_{xy}(z) = -\mathbf{P}_{12}(z,0) \cdot \left(\mathbf{P}_{22}(d,0) + \mathbf{W}^{-1} \cdot \mathbf{P}_{12}(d,0)\right)^{-1} \cdot \eta_0 \boldsymbol{J}_S \tag{3.4}$$

and

$$\eta_0 \mathbf{J} \cdot \boldsymbol{H}_{xy}(z) = -\mathbf{P}_{22}(z,0) \cdot \left(\mathbf{P}_{22}(d,0) + \mathbf{W}^{-1} \cdot \mathbf{P}_{12}(d,0)\right)^{-1} \cdot \eta_0 \boldsymbol{J}_S \tag{3.5}$$

The field above the patch, $z > d$, is, see (3.2)

$$\boldsymbol{E}_{xy}(z) = -\mathbf{P}_{12}(d,0) \cdot \left(\mathbf{P}_{22}(d,0) + \mathbf{W}^{-1} \cdot \mathbf{P}_{12}(d,0)\right)^{-1} \cdot \eta_0 \boldsymbol{J}_S \mathrm{e}^{\mathrm{i}k_z(z-d)} \tag{3.6}$$

and

$$\eta_0 \mathbf{J} \cdot \boldsymbol{H}_{xy}(z) = \mathbf{W}^{-1} \cdot \mathbf{P}_{12}(d,0) \cdot \left(\mathbf{P}_{22}(d,0) + \mathbf{W}^{-1} \cdot \mathbf{P}_{12}(d,0)\right)^{-1} \cdot \eta_0 \boldsymbol{J}_S \mathrm{e}^{\mathrm{i}k_z(z-d)} \tag{3.7}$$

These equations are the basic equations for a Method of Moment (MoM) formulation. To see this, expand the surface current density $\boldsymbol{J}_S(\boldsymbol{\rho})$ in a complete set of expansion functions, $\boldsymbol{j}_n(\boldsymbol{\rho})$, *i.e.*,

$$\boldsymbol{J}_S(\boldsymbol{\rho}) = \sum_n \alpha_n \boldsymbol{j}_n(\boldsymbol{\rho})$$

Note that this is an expansion of the surface current density in the physical domain. The Fourier transform w.r.t. $\boldsymbol{\rho}$ is

$$\boldsymbol{J}_S(\boldsymbol{k}_t) = \sum_n \alpha_n \boldsymbol{j}_n(\boldsymbol{k}_t)$$

Let $\boldsymbol{w}_n(\boldsymbol{\rho})$ be any vector-valued weight-function whose support is contained on the patch. In the Galerkin's method we use

$$\boldsymbol{w}_n(\boldsymbol{\rho}) = \begin{cases} \mathbf{0} & \text{outside the patch} \\ \boldsymbol{j}_n(\boldsymbol{\rho}) & \text{on the patch} \end{cases}$$

Then, due to the boundary conditions on the patch, $\boldsymbol{E}_{xy}(\boldsymbol{\rho}, d) = \mathbf{0}$ on the patch

$$\iint_{-\infty}^{\infty} \boldsymbol{w}_n(\boldsymbol{\rho})^* \cdot \boldsymbol{E}_{xy}(\boldsymbol{\rho}, d) \, \mathrm{d}x \, \mathrm{d}y = 0$$

Using the Parseval theorem gives the result

$$\int_{-\infty}^{\infty}\!\!\int \boldsymbol{w}_n(\boldsymbol{k}_t)^* \cdot \boldsymbol{E}_{xy}(\boldsymbol{k}_t, d)\ \mathrm{d}k_x\ \mathrm{d}k_y = 0$$

in which equation (3.6) can be substituted and a system of equations of the form $\mathbf{A} \cdot \boldsymbol{\alpha} = \boldsymbol{b}$ for the unknown α_n is obtained. The vector $\boldsymbol{b}$ contains the impressed sources of the problem and the matrix $\mathbf{A}$ is

$$\mathbf{A}_{nn'} = \int_{-\infty}^{\infty}\!\!\int \boldsymbol{w}_n(\boldsymbol{k}_t)^* \cdot \mathbf{P}_{12}(\boldsymbol{k}_t, d, 0) \cdot \left(\mathbf{P}_{22}(\boldsymbol{k}_t, d, 0) + \mathbf{W}^{-1}(\boldsymbol{k}_t) \cdot \mathbf{P}_{12}(\boldsymbol{k}_t, d, 0)\right)^{-1} \cdot \boldsymbol{j}_{n'}(\boldsymbol{k}_t)\ \mathrm{d}k_x\ \mathrm{d}k_y$$

Since a full MoM solution of the problem is outside of the scope of this paper, we do not pursue the MoM approach any further here, but refer to the literature for additional details, see *e.g.*, [42]. The matrix $\mathbf{A}_{nn'}$ also determines the resonance frequencies of the antenna and its bandwidth [7, 8, 26–29].

As pointed out above, the propagator $\mathbf{P}_{ij}(\boldsymbol{k}_t, z, 0)$ are analytic dyadics in the parameter $\boldsymbol{k}_t$. The same analytic properties then hold for the fields $\boldsymbol{E}_{xy}(\boldsymbol{k}_t, z)$ and $\boldsymbol{H}_{xy}(\boldsymbol{k}_t, z)$ for all z values, with the exceptions of the discrete values of $\boldsymbol{k}_t$ which correspond to zero eigenvalues of the dyadic $\mathbf{P}_{22}(\boldsymbol{k}_t, d, 0) + \mathbf{W}^{-1}(\boldsymbol{k}_t) \cdot \mathbf{P}_{12}(\boldsymbol{k}_t, d, 0)$.

The result in this section can easily be compared with the result in Appendix C, which employes the traditional technique with reflection dyadic, which is defined in (C.2). The reflection dyadic of the grounded substrate expressed in the propagator formulation is [35][2]

$$\begin{aligned}\mathbf{r} =& \left(\mathbf{P}_{12}(d,0) - \mathbf{W} \cdot \mathbf{P}_{22}(d,0)\right) \cdot \left(\mathbf{P}_{12}(d,0) + \mathbf{W} \cdot \mathbf{P}_{22}(d,0)\right)^{-1} \\ =& \mathbf{W} \cdot \left(\mathbf{W}^{-1} \cdot \mathbf{P}_{12}(d,0) - \mathbf{P}_{22}(d,0)\right) \cdot \left(\mathbf{W}^{-1} \cdot \mathbf{P}_{12}(d,0) + \mathbf{P}_{22}(d,0)\right)^{-1} \cdot \mathbf{W}^{-1}\end{aligned} \tag{3.8}$$

This observation implies, see (3.3)

$$\boldsymbol{F}^+(d^+) = -\frac{1}{2}\left(\mathbf{I}_2 + \mathbf{r}\right) \cdot \mathbf{W} \cdot \eta_0 \boldsymbol{J}_S$$

since

$$\mathbf{I}_2 + \mathbf{r} = 2\mathbf{P}_{12}(d,0) \cdot \left(\mathbf{P}_{12}(d,0) + \mathbf{W} \cdot \mathbf{P}_{22}(d,0)\right)^{-1}$$

This result is identical to (C.4).

4 Surface waves

From the solution of the field quantities in the spectral domain, *i.e.*, $\boldsymbol{E}_{xy}(\boldsymbol{k}_t, z)$ and $\boldsymbol{H}_{xy}(\boldsymbol{k}_t, z)$, we obtain the fields at point $\boldsymbol{r}$ in space by an inverse Fourier transform,

[2]The results of Ref. 35 have to be modified to fit with the approach used in this paper, *e.g.*, the results in [35] use the inverses of the propagators given here.

see (2.2). Above, we concluded that the fields in the spectral domain are analytic functions of $\boldsymbol{k}_t$ for all values of z, except at possible singularities at those $\boldsymbol{k}_t$-values where we have a zero eigenvalue of the dyadic $\mathbf{P}_{22}(d,0) + \mathbf{W}^{-1} \cdot \mathbf{P}_{12}(d,0)$. These $\boldsymbol{k}_t$-values are pole contributions, and they determine the surface modes that might be present in the problem. The relation between these $\boldsymbol{k}_t$-values and the angular frequency ω defines the dispersion relation of the surface wave.

An alternative way of determining these surface modes is to search for the $\boldsymbol{k}_t$-values at which the reflection dyadic, $\mathbf{r}$, is singular, see (3.8), or, as the $\boldsymbol{k}_t$-values at which $\mathbf{r}^{-1}$ have zero eigenvalues. From the relation $\boldsymbol{F}^-(z=d^-) = \mathbf{r}^{-1} \cdot \boldsymbol{F}^+(z=d^-)$, we then see that these cases correspond to a situation where $\boldsymbol{F}^+(z=d^-) \neq \mathbf{0}$ and $\boldsymbol{F}^-(z=d^-) = \mathbf{0}$. Several ways of calculating $\mathbf{r}^{-1}$ are presented in Appendix D.

The $\boldsymbol{k}_t$-values of the surface waves for an inhomogeneous, isotropic material have to be found in a numerical search, where the propagators are obtained by the solution of the ODEs in (2.9)–(2.10). The homogeneous case, which is a case where the explicit equations can easily be found, is analyzed in Appendix E.

The frequency at which a new surface wave appears is the onset of the surface wave, and to determine this frequency is the aim of the section below.

4.1 The onset of surface waves

The $k_0 d$-value, *i.e.*, the angular frequency ω (appropriately normalized), that determines the onset of the surface wave is analyzed in this section.

For an isotropic material, the $\boldsymbol{k}_t$-value for onset is $k_t = k_0$, or stated differently $k_z = 0$ at this frequency. Therefore, the condition for the onset of a surface mode, $\det(\mathbf{P}_{22} + \mathbf{W}^{-1} \cdot \mathbf{P}_{12}) = 0$, is different for the TM- and the TE-cases. At onset, due to (2.16), $\det(\mathbf{P}_{22} + \mathbf{W}^{-1} \cdot \mathbf{P}_{12}) = 0$ then simplifies to

$$\begin{cases} P_{12}^{\mathrm{TM}}(k_t = k_0, d, 0) = 0, & \text{TM-case} \\ P_{22}^{\mathrm{TE}}(k_t = k_0, d, 0) = 0, & \text{TE-case} \end{cases} \tag{4.1}$$

The propagators for this special value on $\boldsymbol{k}_t$ are determined by

$$\begin{cases} \dfrac{\mathrm{d}}{\mathrm{d}z}\mathbf{P}_{12}(\boldsymbol{k}_t, z, 0) = \mathrm{i}k_0 \mathbf{M}_{12}(\boldsymbol{k}_t, z) \cdot \mathbf{P}_{22}(\boldsymbol{k}_t, z, 0) \\ \dfrac{\mathrm{d}}{\mathrm{d}z}\mathbf{P}_{22}(\boldsymbol{k}_t, z, 0) = \mathrm{i}k_0 \mathbf{M}_{21}(\boldsymbol{k}_t, z) \cdot \mathbf{P}_{12}(\boldsymbol{k}_t, z, 0) \end{cases}, \qquad \boldsymbol{k}_t = k_0 \hat{\boldsymbol{e}}_{\parallel}$$

which follows directly from (2.9)–(2.10). The explicit ODEs for the TM- and TE-cases are also readily found. The result is, see (2.11) and (2.12)

$$\begin{cases} \dfrac{\mathrm{d}}{\mathrm{d}z}P_{12}^{\mathrm{TM}} = \mathrm{i}k_0 \left(\dfrac{1}{\epsilon(z)} - \mu(z) \right) P_{22}^{\mathrm{TM}} \\ \dfrac{\mathrm{d}}{\mathrm{d}z}P_{22}^{\mathrm{TM}} = -\mathrm{i}k_0 \epsilon(z) P_{12}^{\mathrm{TM}} \end{cases} \qquad \begin{cases} P_{12}^{\mathrm{TM}}(0,0) = 0 \\ P_{22}^{\mathrm{TM}}(0,0) = 1 \end{cases}$$

and

$$\begin{cases} \dfrac{\mathrm{d}}{\mathrm{d}z}P_{12}^{\mathrm{TE}} = -\mathrm{i}k_0\mu(z)P_{22}^{\mathrm{TE}} \\ \dfrac{\mathrm{d}}{\mathrm{d}z}P_{22}^{\mathrm{TE}} = \mathrm{i}k_0\left(\dfrac{1}{\mu(z)} - \epsilon(z)\right)P_{12}^{\mathrm{TE}} \end{cases} \qquad \begin{cases} P_{12}^{\mathrm{TE}}(0,0) = 0 \\ P_{22}^{\mathrm{TE}}(0,0) = 1 \end{cases}$$

To find the onset frequency, these special versions of the propagator equations are solved numerically and evaluated at $z = d$. The frequency value that satisfies (4.1) then determines the onset of the surface mode. The modes are labeled as TM_n and TE_n, $n = 1, 2, \ldots$, and ordered in increasing values of the onset frequency. In addition to these modes there always exists a mode TM_0 for all frequency (zero cut-off frequency) for this type of geometry.

For an homogenous profile the onset frequencies determined by (4.1) are explicitly given by, see (E.1) and (E.2)

$$\begin{cases} k_0 d = \dfrac{n\pi}{\sqrt{\epsilon\mu - 1}}, & \text{TM-case} \\ k_0 d = \dfrac{(2n+1)\pi}{2\sqrt{\epsilon\mu - 1}}, & \text{TE-case} \end{cases} \qquad n = 0, 1, 2, 3, \ldots \tag{4.2}$$

4.2 Numerical examples

In a series of numerical examples, we illustrate the dispersion of the surface waves for a collection of grounded, inhomogeneous substrates. The differences and the similarities between the results are also briefly discussed.

The relative permittivity profiles of interest in this paper are:

$$\begin{cases} \epsilon(z) = 2 + 8z^2/d^2 & \text{Profile 1), Quadratic profile} \\ \epsilon(z) = 2 + 8\left(d - z\right)^2/d^2 & \text{Profile 2), Reverse quadratic profile} \\ \epsilon(z) = 10 - 8z^2/d^2 & \text{Profile 3), Decreasing quadratic profile} \\ \epsilon(z) = 2 + 2e^{-(z/d-0.6)^2/0.1^2} & \text{Profile 4), Increasing Gaussian profile} \\ \epsilon(z) = 4 - 2e^{-(z/d-0.6)^2/0.1^2} & \text{Profile 5), Decreasing Gaussian profile} \\ \epsilon(z) = 8/(4 - 2z/d) & \text{Profile 6), Reciprocal profile} \\ \epsilon(z) = 8/(4 - 2\left(d - z\right)/d) & \text{Profile 7), Reverse reciprocal profile} \\ \epsilon(z) = \begin{cases} 2 & 0 \le z/d \le 0.9 \\ 10 & 0.9 \le z/d \le 1 \end{cases} & \text{Profile 8), Step discontinous profile} \end{cases} \tag{4.3}$$

In all profiles the relative permeability $\mu(z) = 1$.

Figure 3 depicts the dispersion curves of the ϵ-profile 1) in (4.3) — an increasing quadratic profile. The upper figure shows the normalized frequency $k_0 d = \omega d/c_0$ as a function of the normalized wave number $k_t d$ of the surface mode. The straight line is the line $k_0 = k_t$, which gives the dispersion curve for a free space wave. We immediately see that all surface modes have a k_t-value that is larger than k_0, and, therefore, the surface wave propagates slower than the corresponding free space wave does [15]. The lower figure shows the corresponding quantities for a homogeneous

profile with a homogenized epsilon value. The homogenized values of the relative permittivity, ϵ_h, and the relative permeability, μ_h, are defined in (2.13). The onset of modes are intertwined as TM_0, TE_1, TM_1, TE_2, *etc.*, but at higher frequencies the curves cross each other. This is not the case for the homogenized profile.

The dispersion curves for the reverse quadratic profile, profile 2) in (4.3), is given in Figure 4. We see that the curves now do not intersect for this profile.

The effective permittivity the surface wave experiences as it propagates is proportional to k_t^2. Note that the effective permittivity is essentially the inverse of the dispersion curves shown above. In Figures 5–9, k_t^2/k_0^2 is depicted for profiles 4)–8) in (4.3) as a function of the normalized thickness $k_0 d$. The same conclusions as we made in Figures 3 and 4 can be made here; profiles with increasing permittivity away from ground have dispersion curves that cross each other, while dispersion curves for decreasing and constant profiles do not.

In all our examples, the material in the substrate has been lossless. If we have losses in the material, there are, in general, no real $\boldsymbol{k}_t$-values that correspond to zero eigenvalues of the dyadic $\mathbf{P}_{22}(d,0) + \mathbf{W}^{-1} \cdot \mathbf{P}_{12}(d,0)$. The surface wave is in these cases exponentially damped in the lateral directions, and it gives no contribution to the radiated power, see Section 6.

5 Radiated power into the half space

The radiated power from the patch antenna is required in order to calculate the radiation efficiency and directivity of the antenna. The radiated power consists of two contributions — one from the space wave and one from the surface wave. In this section, we calculate the space wave contribution, and the surface wave is found in Section 6.

As an approximation of the correct surface current density on the patch antenna, *i.e.*, the sum of the surface current densities on both sides of the patch, we make the assumption that the surface current density is approximated by the lowest order eigenmode that is used in a numerical scheme, *e.g.*, Method of Moments, or the equivalent surface current density on the patch in analogy with the cavity model approach [3]. Numerical experiments show that additional higher-order basis functions lead to negligible changes in the results near the first resonance [42]. Of course, out-of-band frequencies or higher order resonances require that more modes are included and that a full MoM calculation is made [7, 8, 26–28, 42].

Below, we give the approximate expressions for the surface current densities on a rectangular and a circular patch.

5.1 Current density on rectangular patch

We assume the surface current density on a rectangular patch, length a (in the x-direction) and width b (in the y-direction), centered at the origin, is given by [3]

$$\boldsymbol{J}_S(\boldsymbol{\rho}) = C\hat{\boldsymbol{x}} \cos\frac{\pi x}{a} \chi_{[-a/2,a/2]}(x)\chi_{[-b/2,b/2]}(y)$$

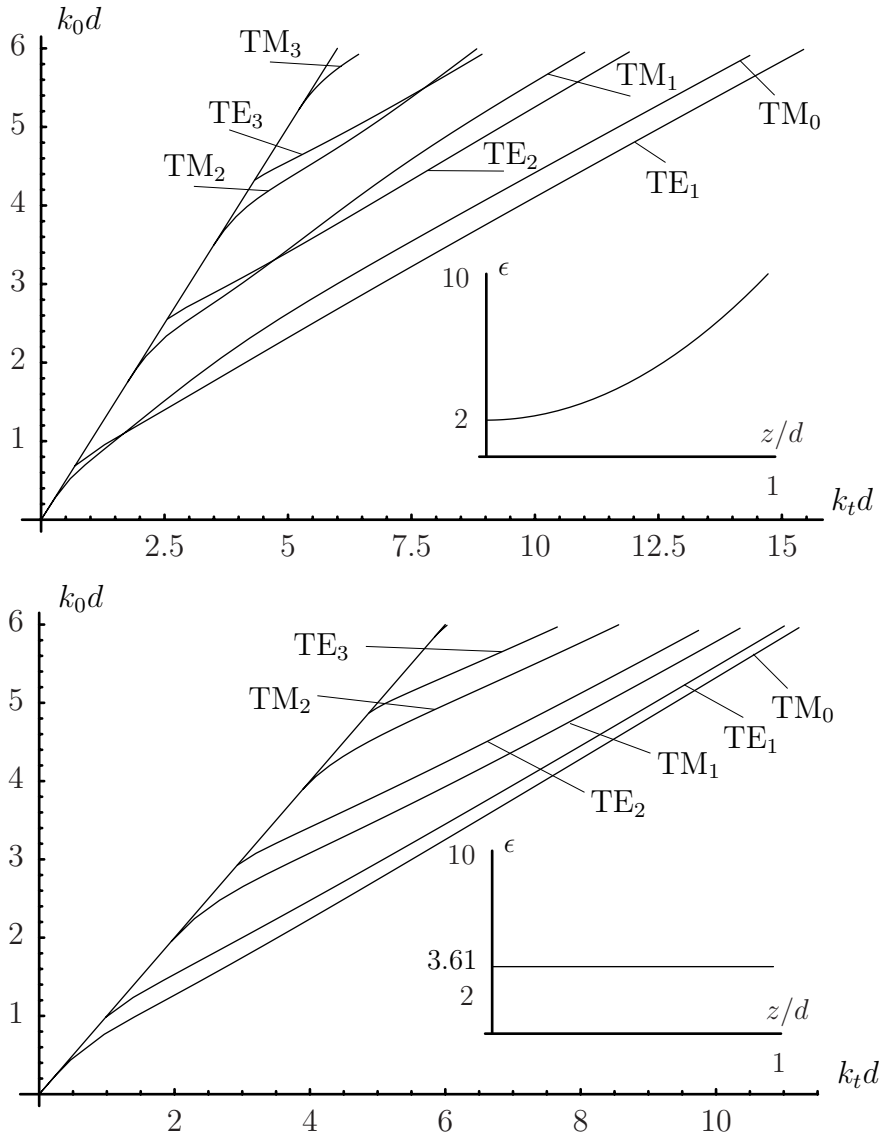

Figure 3: The normalized frequency $k_0d = \omega d/c_0$ as a function of the normalized wave number k_td of the surface mode. The upper figure shows the dispersion curves for ϵ-profile 1) in (4.3), and the lower figure shows the corresponding quantities for the homogenized profile. The k_0d-values for the onset of the different modes for the inhomogeneous profile are: TM$_0$ = 0, TE$_1$ = 0.677, TM$_1$ = 1.74, TE$_2$ = 2.54, TM$_2$ = 3.48, TE$_3$ = 4.31, and TM$_3$ = 5.21. The corresponding onset values for the homogenized profile are given by (4.2) with $\epsilon_h = 3.61$.

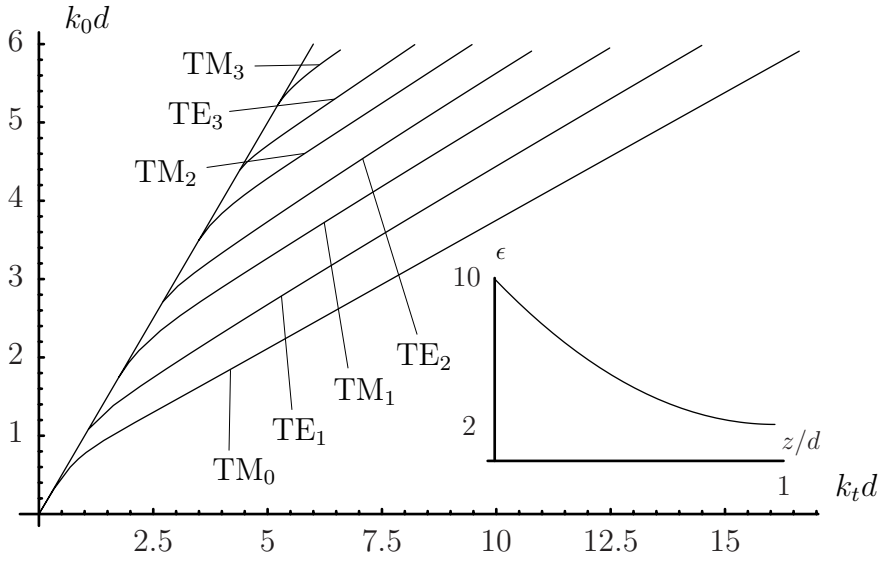

Figure 4: The normalized frequency $k_0d = \omega d/c_0$ as a function of the normalized wave number k_td of the surface mode. The figure shows the dispersion curves for ϵ-profile 2) in (4.3). The k_0d-values for the onset of the different modes for the inhomogeneous profile are: $\mathrm{TM}_0 = 0$, $\mathrm{TE}_1 = 1.07$, $\mathrm{TM}_1 = 1.74$, $\mathrm{TE}_2 = 2.70$, $\mathrm{TM}_2 = 3.48$, $\mathrm{TE}_3 = 4.38$, and $\mathrm{TM}_3 = 5.21$. The homogenized profile is identical to the one in Figure 3.

where the characteristic function of an interval I is denoted $\chi_I(x)$, *i.e.*, $\chi(x) = 1$ if $x \in I$, and zero otherwise. In a cavity model approach this corresponds to a TM_{100}-mode [3]. C is an appropriate constant.

The Fourier transform of this surface current density is

$$\begin{aligned}\boldsymbol{J}_S(\boldsymbol{k}_t) =& -2\pi abC\hat{\boldsymbol{x}}\frac{\cos k_x a/2}{k_x^2a^2-\pi^2}\mathrm{sinc}\frac{k_yb}{2}\\ =&2abC\left[\mathrm{sinc}\frac{k_xa+\pi}{2}+\mathrm{sinc}\frac{k_xa-\pi}{2}\right]\mathrm{sinc}\frac{k_yb}{2}\left(\hat{\boldsymbol{e}}_\parallel\cos\alpha-\hat{\boldsymbol{e}}_\perp\sin\alpha\right)\end{aligned}$$

where $\cos\alpha = \hat{\boldsymbol{e}}_\parallel \cdot \hat{\boldsymbol{x}}$. An approximate value of the resonance frequency in a homogeneous, isotropic substrate is [3, 24]

$$f_r = \frac{c_0}{2a\sqrt{\epsilon\mu}} \tag{5.1}$$

5.2 Current density on circular patch

The assumptions of surface current density on the circular patch are similar to the rectangular patch above. The radius of the patch is a. The surface current density is assumed to be given by [3]

$$\boldsymbol{J}_S(\boldsymbol{\rho}) = C\left[2\hat{\boldsymbol{\rho}}J_1'(\eta_{11}\rho/a)\cos\phi - \frac{2a}{\eta_{11}}\hat{\boldsymbol{\phi}}\frac{J_1(\eta_{11}\rho/a)}{\rho}\sin\phi\right]$$

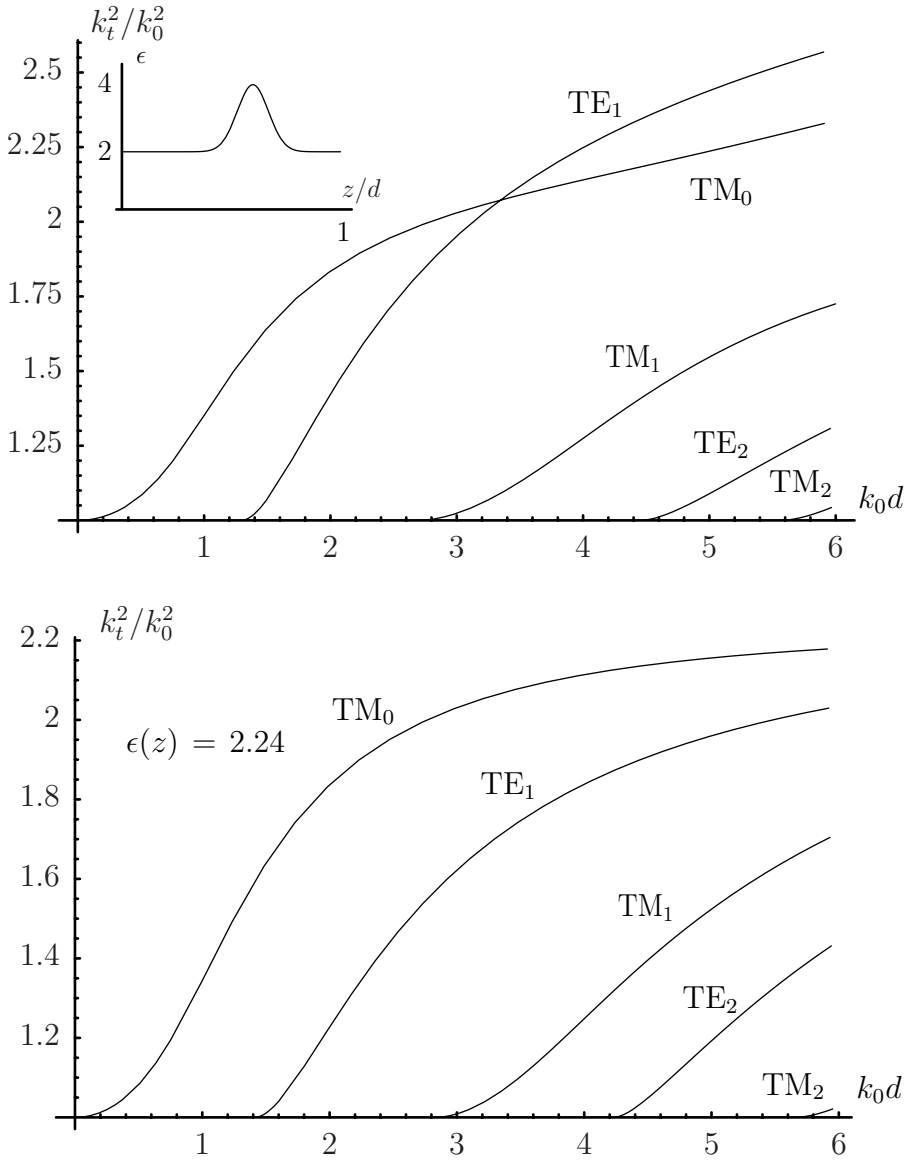

Figure 5: The wave number k_t^2 (scaled with k_0^2) for the surface mode as a function of the thickness k_0d for ϵ-profile 4) in (4.3), and the lower figure shows the corresponding quantities for the homogenized profile. The k_0d-values for the onset of the different modes for the inhomogeneous profile are: $\mathrm{TM}_0 = 0$, $\mathrm{TE}_1 = 1.29$, $\mathrm{TM}_1 = 2.67$, $\mathrm{TE}_2 = 4.45$, and $\mathrm{TM}_2 = 5.56$. The corresponding onset values for the homogenized profile are given by (4.2) with $\epsilon_h = 2.24$.

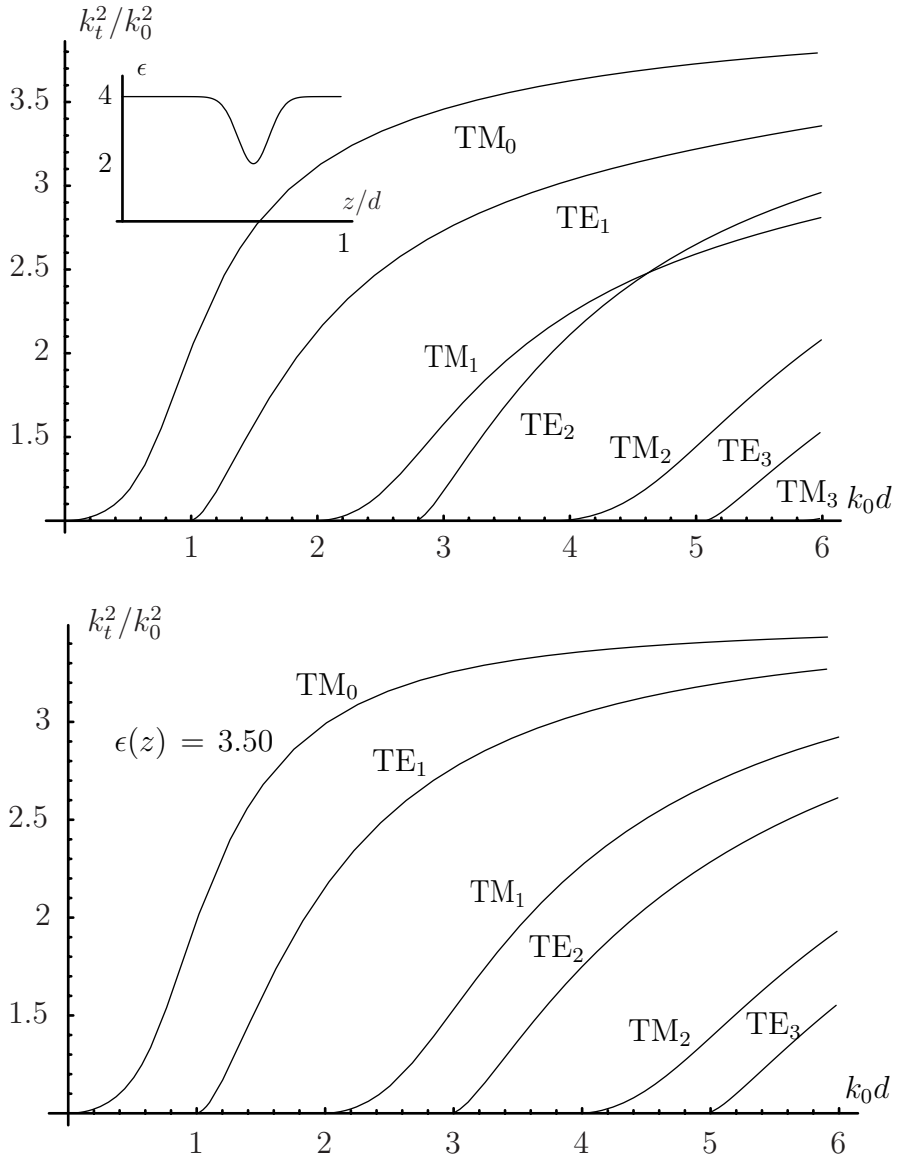

Figure 6: The wave number k_t^2 (scaled with k_0^2) for the surface mode as a function of the thickness k_0d for ϵ-profile 5) in (4.3), and the lower figure shows the corresponding quantities for the homogenized profile. The k_0d-values for the onset of the different modes for the inhomogeneous profile are: $\mathrm{TM}_0 = 0$, $\mathrm{TE}_1 = 0.985$, $\mathrm{TM}_1 = 1.98$, $\mathrm{TE}_2 = 2.78$, $\mathrm{TM}_2 = 3.88$, $\mathrm{TE}_3 = 5.07$, and $\mathrm{TM}_3 = 5.82$. The corresponding onset values for the homogenized profile are given by (4.2) with $\epsilon_h = 2.24$.

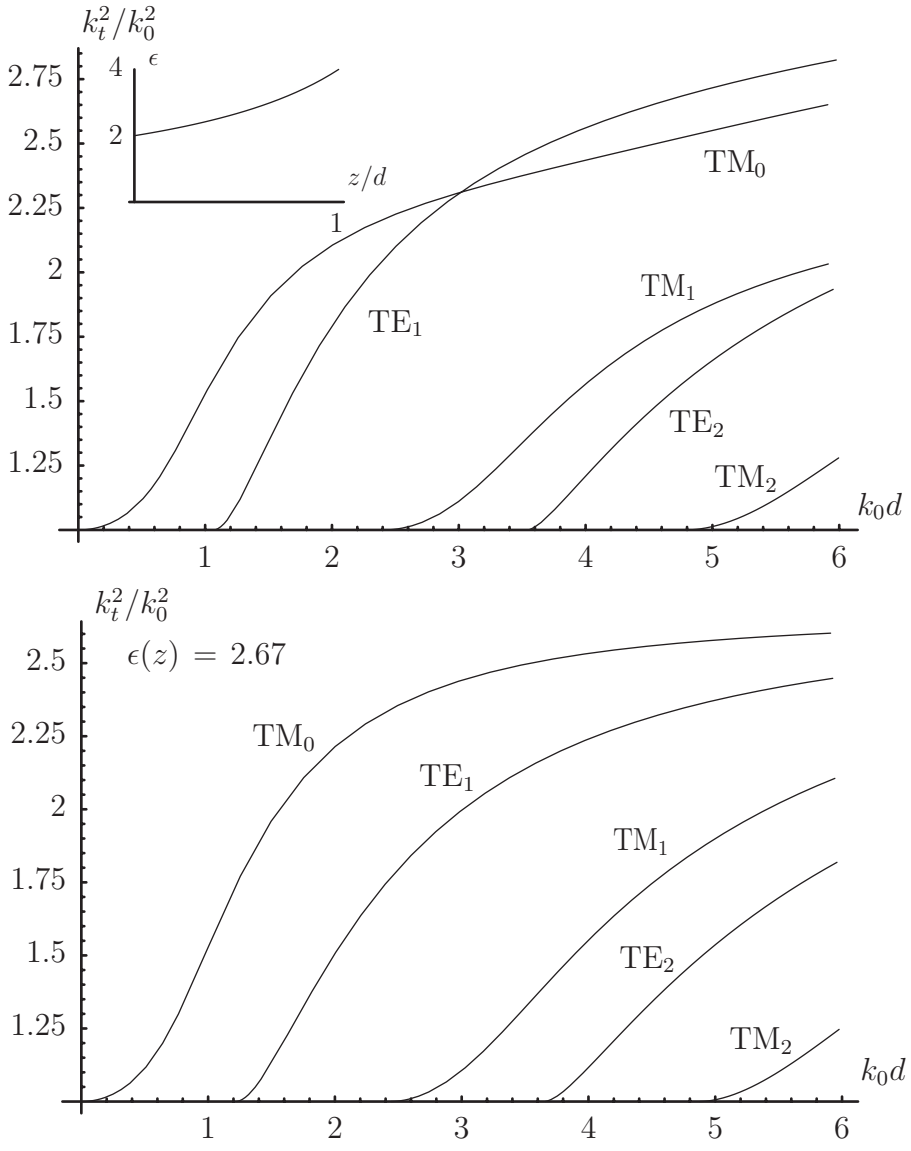

Figure 7: The wave number k_t^2 (scaled with k_0^2) for the surface mode as a function of the thickness k_0d for ϵ-profile 6) in (4.3), and the lower figure shows the corresponding quantities for the homogenized profile. The k_0d-values for the onset of the different modes for the inhomogeneous profile are: $\mathrm{TM}_0 = 0$, $\mathrm{TE}_1 = 1.07$, $\mathrm{TM}_1 = 2.40$, $\mathrm{TE}_2 = 3.54$, $\mathrm{TM}_2 = 4.79$, and $\mathrm{TE}_3 = 5.95$. The corresponding onset values for the homogenized profile are given by (4.2) with $\epsilon_h = 2.67$.

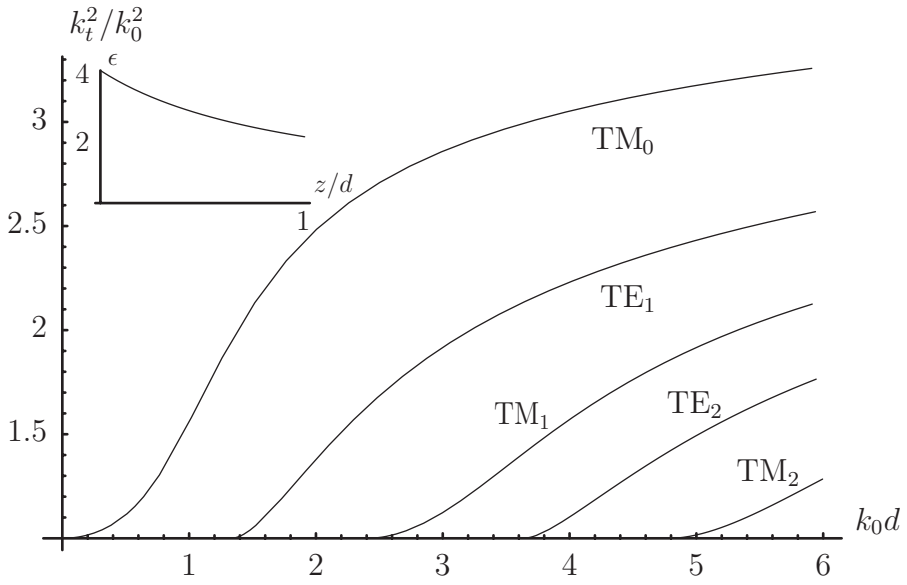

Figure 8: The wave number k_t^2 (scaled with k_0^2) for the surface mode as a function of the thickness $k_0 d$ for ϵ-profile 7) in (4.3). The $k_0 d$-values for the onset of the different modes for the inhomogeneous profile are: $\mathrm{TM}_0 = 0$, $\mathrm{TE}_1 = 1.33$, $\mathrm{TM}_1 = 2.40$, $\mathrm{TE}_2 = 3.63$, and $\mathrm{TM}_2 = 4.79$. The homogenized profile is identical to the one in Figure 7.

where $\eta_{11} \approx 1.841$ and where $\rho = \sqrt{x^2 + y^2}$ and ϕ is the azimuth angle in the x-y-plane. This corresponds to a TM_{110}-mode in a cavity model approach. C is an appropriate constant. The current is oriented along the $\hat{\boldsymbol{x}}$-axis close to the origin. In fact, we have

$$\boldsymbol{J}_S(\boldsymbol{\rho} = \boldsymbol{0}) = C\hat{\boldsymbol{x}}$$

The Fourier transform is [1, 22]

$$\boldsymbol{J}_S(\boldsymbol{k}_t) = \frac{4\pi C a^2 J_1(\eta_{11})}{\eta_{11}} \left\{ \hat{\boldsymbol{e}}_{\parallel} \frac{\eta_{11}^2 J_1'(k_t a)}{\eta_{11}^2 - k_t^2 a^2} \cos\alpha - \hat{\boldsymbol{e}}_{\perp} \frac{J_1(k_t a)}{k_t a} \sin\alpha \right\} \tag{5.2}$$

This mode has the lowest cutoff frequency and an approximate value of the resonance frequency in a homogeneous, isotropic substrate is [3, 7, 8, 14, 24, 36, 44]

$$f_r = \frac{1.841 c_0}{2\pi a \sqrt{\epsilon\mu}} \tag{5.3}$$

5.3 Power flow

The far field amplitude $\boldsymbol{F}(\hat{\boldsymbol{r}})$ of the electric field is

$$\boldsymbol{E}(\boldsymbol{r}) = \boldsymbol{F}(\hat{\boldsymbol{r}}) \frac{e^{ik_0 r}}{k_0 r}, \text{ as } r \to \infty$$

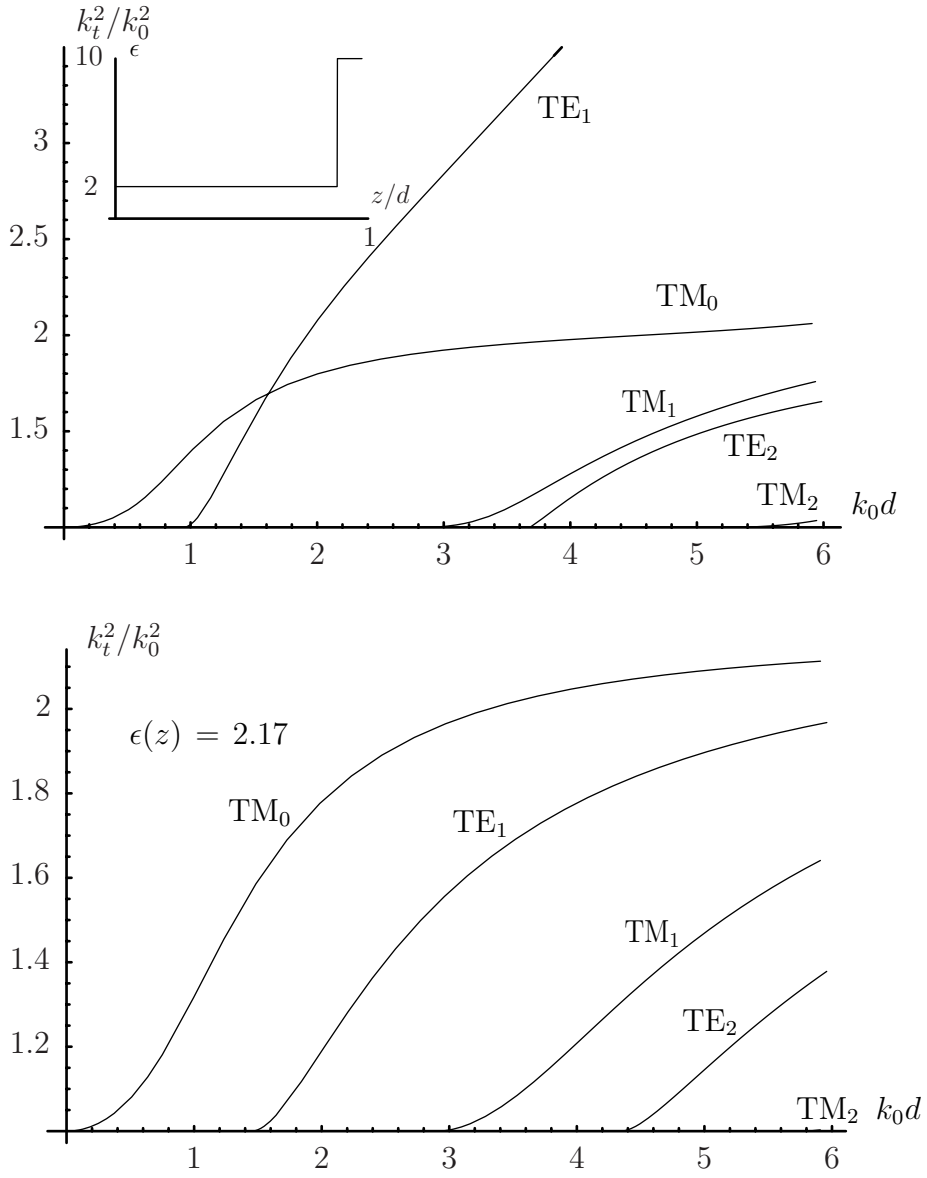

Figure 9: The wave number k_t^2 (scaled with k_0^2) for the surface mode as a function of the thickness k_0d for ϵ-profile 8) in (4.3), and the lower figure shows the corresponding quantities for the homogenized profile. The k_0d-values for the onset of the different modes for the inhomogeneous profile are: $\mathrm{TM}_0 = 0$, $\mathrm{TE}_1 = 0.946$, $\mathrm{TM}_1 = 2.83$, $\mathrm{TE}_2 = 3.68$, and $\mathrm{TM}_2 = 5.24$. The corresponding onset values for the homogenized profile are given by (4.2) with $\epsilon_h = 2.17$.

where the far field amplitude $\boldsymbol{F}(\hat{\boldsymbol{r}})$ is related to the Fourier transform of the electric field at $z = d^+$ as [11, 22] (θ is the polar angle in spherical coordinates, *i.e.*, $\cos\theta = \hat{\boldsymbol{r}} \cdot \hat{\boldsymbol{z}}$)

$$\boldsymbol{F}(\hat{\boldsymbol{r}}) = \mathrm{i}\frac{k_0^2}{2\pi}\hat{\boldsymbol{r}} \times \left[\hat{\boldsymbol{z}} \times \boldsymbol{E}_{xy}(\boldsymbol{k}_t, d^+)\big|_{\boldsymbol{k}_t = k_0 \sin\theta\hat{\boldsymbol{\rho}}}\, e^{-\mathrm{i}k_0 d\cos\theta}\right], \qquad \cos\theta > 0$$

or expressed in the components of the total electric field[3]

$$\boldsymbol{F}(\hat{\boldsymbol{r}}) = -\mathrm{i}\frac{k_0^2}{2\pi}\cos\theta\ \boldsymbol{E}(\boldsymbol{k}_t, d^+)\big|_{\boldsymbol{k}_t = k_0 \sin\theta\hat{\boldsymbol{\rho}}}\, e^{-\mathrm{i}k_0 d\cos\theta}, \qquad \cos\theta > 0$$

The radiated power density in a given direction $\hat{\boldsymbol{r}}$ is given as the modulus of the Pointing vector $\boldsymbol{S}$.

$$|< \boldsymbol{S}(\hat{\boldsymbol{r}}) >| = \left|\frac{1}{2}\,\mathrm{Re}\,\boldsymbol{E}(\boldsymbol{r}) \times \boldsymbol{H}(\boldsymbol{r})^*\right| = \frac{|\boldsymbol{F}(\hat{\boldsymbol{r}})|^2}{2\eta_0 k_0^2 r^2}$$

where $|\boldsymbol{A}|^2 = \boldsymbol{A} \cdot \boldsymbol{A}^*$.

The transverse electric field $\boldsymbol{E}_{xy}$ above the patch contains only one split component, *i.e.*, the wave splitting implies $\boldsymbol{E}_{xy}(\boldsymbol{k}_t, z) = \boldsymbol{F}^+(\boldsymbol{k}_t, z)$. We have

$$\begin{aligned}|\boldsymbol{F}(\hat{\boldsymbol{r}})|^2 &= \frac{k_0^4}{4\pi^2}\left|\hat{\boldsymbol{r}} \times \left[\hat{\boldsymbol{z}} \times \boldsymbol{E}_{xy}(\boldsymbol{k}_t = k_0 \sin\theta\hat{\boldsymbol{\rho}}, d^+)\right]\right|^2 \\ &= \frac{k_0^4}{4\pi^2}\left|\hat{\boldsymbol{z}}\sin\theta\left(\hat{\boldsymbol{\rho}} \cdot \boldsymbol{F}^+(\boldsymbol{k}_t, d^+)\right) - \boldsymbol{F}^+(\boldsymbol{k}_t, d^+)\cos\theta\right|^2_{\boldsymbol{k}_t = k_0 \sin\theta\hat{\boldsymbol{\rho}}}\end{aligned}$$

where relations between the spherical and cylindric coordinate systems has been used. The final expression for the radiated power density expressed in the split field $\boldsymbol{F}^+$ is

$$|< \boldsymbol{S}(\hat{\boldsymbol{r}}) >| = \frac{k_0^2}{8\pi^2\eta_0 r^2}\left(\left|\boldsymbol{F}^+(\boldsymbol{k}_t, d^+) \cdot \hat{\boldsymbol{e}}_{\parallel}\right|^2 + \left|\boldsymbol{F}^+(\boldsymbol{k}_t, d^+) \cdot \hat{\boldsymbol{e}}_{\perp}\right|^2 \cos^2\theta\right)_{\boldsymbol{k}_t = k_0 \sin\theta\hat{\boldsymbol{\rho}}}$$

where the orthogonality between $\boldsymbol{F}^+$ and $\hat{\boldsymbol{z}}$ has been used. The field $\boldsymbol{F}^+(\boldsymbol{k}_t, d^+)$ is given by the expression in (3.3), *i.e.*,

$$\boldsymbol{F}^+(\boldsymbol{k}_t, d^+) = -\mathbf{P}_{12}(\boldsymbol{k}_t, d, 0) \cdot \left(\mathbf{P}_{22}(\boldsymbol{k}_t, d, 0) + \mathbf{W}^{-1} \cdot \mathbf{P}_{12}(\boldsymbol{k}_t, d, 0)\right)^{-1} \cdot \eta_0 \boldsymbol{J}_S(\boldsymbol{k}_t)$$

The power radiated in the upper half space is obtained by an integration over the unit sphere in the upper half space, *i.e.*,

$$P_{\mathrm{r}} = \int_0^{\pi/2} \mathrm{d}\theta \int_0^{2\pi} \mathrm{d}\phi\ r^2 \sin\theta\, |< \boldsymbol{S}(\hat{\boldsymbol{r}}) >| \tag{5.4}$$

[3]The total electric field in a region where only the $\boldsymbol{F}^+$ field contributes is (2.6)

$$\boldsymbol{E}(\boldsymbol{k}_t, z) = \boldsymbol{E}_{xy}(\boldsymbol{k}_t, z) + \hat{\boldsymbol{z}}\frac{\eta_0}{k_0}\boldsymbol{k}_t \cdot \mathbf{J} \cdot \boldsymbol{H}_{xy}(\boldsymbol{k}_t, z) = \boldsymbol{E}_{xy}(\boldsymbol{k}_t, z) - \hat{\boldsymbol{z}}\frac{1}{k_0}\boldsymbol{k}_t \cdot \mathbf{W}^{-1} \cdot \boldsymbol{E}_{xy}(\boldsymbol{k}_t, z)$$

or

$$\begin{aligned}\cos\theta\boldsymbol{E}(k_0 \sin\theta\hat{\boldsymbol{\rho}}, z) &= \cos\theta\boldsymbol{E}_{xy}(k_0 \sin\theta\hat{\boldsymbol{\rho}}, z) - \hat{\boldsymbol{z}}\sin\theta\hat{\boldsymbol{\rho}} \cdot \boldsymbol{E}_{xy}(k_0 \sin\theta\hat{\boldsymbol{\rho}}, z) \\ &= -\hat{\boldsymbol{r}} \times \left[\hat{\boldsymbol{z}} \times \boldsymbol{E}_{xy}(\boldsymbol{k}_t, z)|_{\boldsymbol{k}_t = k_0 \sin\theta\hat{\boldsymbol{\rho}}}\right]\end{aligned}$$

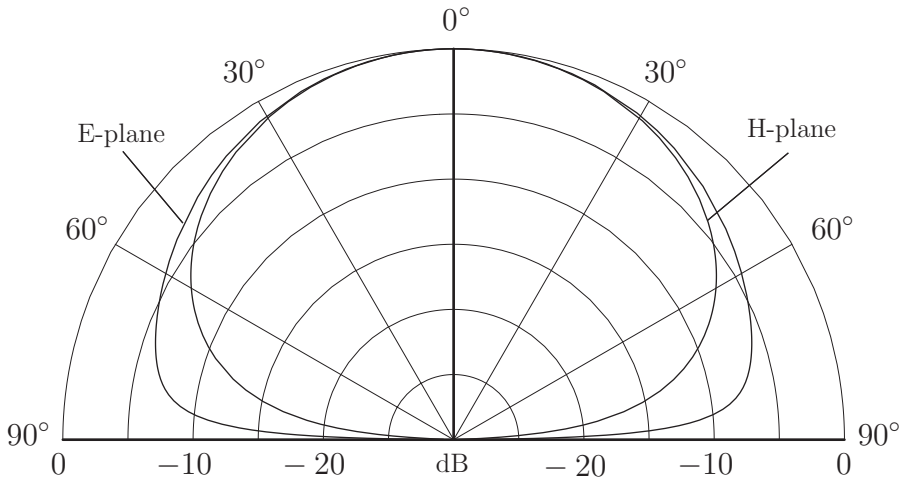

Figure 10: The radiation pattern of a rectangular patch antenna (length a and width $b = 0.8a$) on a dielectric slab (permittivity profile 4) in (4.3)). The thickness of the substrate is $d = 0.1a$.

From the equations above, it is not hard to derive the leading behavior of the radiated power in terms of the parameter $k_0 d$. The result is $P_{\rm r} = O((k_0 d)^2)$.

The radiation diagram of a patch antenna on a grounded, inhomogeneous substrate can easily be found by numerical integration. A numerical example of the radiation pattern of a rectangular patch on an inhomogeneous permittivity profile (profile 4) in (4.3)), is given in Figure 10. The patch has length a and width $b = 0.8a$. The resonance frequency for the patch is approximated by, see (5.1)

$$k_0 a = \frac{\pi}{\sqrt{\epsilon_h \mu_h}}$$

where the homogenized values of the relative permittivity and the relative permeability, ϵ_h and μ_h, respectively, are defined in (2.13). The thickness of the substrate is $d = 0.1a$.

For a circular patch, the radiation pattern for two profiles are shown in Figure 11. The relation between the radius a of the patch and the resonance frequency is approximated by (5.3), *i.e.*,

$$k_0 a = \frac{1.841}{\sqrt{\epsilon_h \mu_h}}$$

We observe that the radiation of the patch on the increasing profile gives a more directed radiation compared to radiation of the patch on the decreasing profile. This is especially true for the radiation in the E-plane.

6 Surface wave power

The main goal with this section is to find an expression of the power radiated by the surface mode in the grounded, inhomogeneous substrate excited by a circular

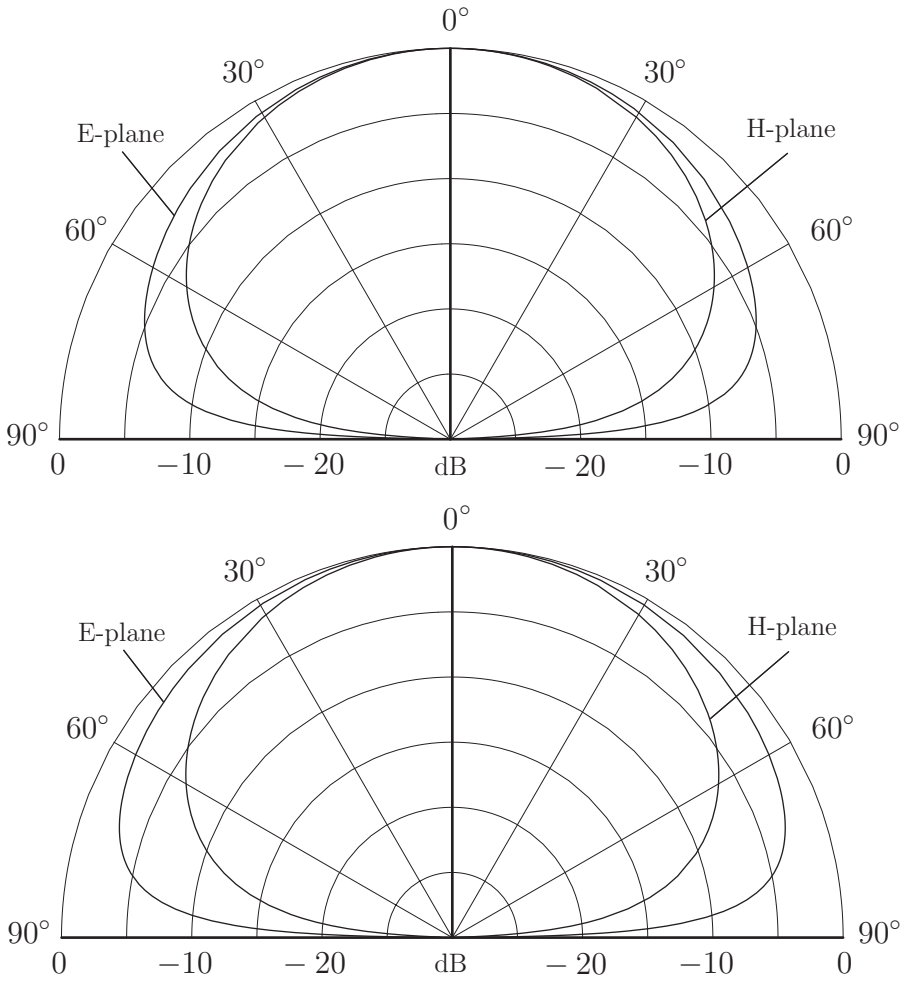

Figure 11: The radiation pattern of a circular patch antenna (radius a) on a dielectric slab. The thickness of the substrate is $d = 0.3a$ and the upper figure shows the radiation pattern for permittivity profile 1) in (4.3)). The lower figure is the corresponding radiation pattern for profile 3).

patch with current distribution $\boldsymbol{J}_S(\boldsymbol{k}_t)$ given by (5.2). We start with the results found in Section 4, where we concluded that the surface modes are determined by the zero eigenvalues of the dyadic $\mathbf{P}_{22}(d,0) + \mathbf{W}^{-1} \cdot \mathbf{P}_{12}(d,0)$. These $\boldsymbol{k}_t$-values are poles of the fields, and located at $\boldsymbol{k}_{t\mathrm{sw}} = k_{t\mathrm{sw}}\hat{\boldsymbol{e}}_{\parallel}$. The only other singularity of the fields are the branch points at $\boldsymbol{k}_{t\mathrm{sw}} = \pm k_0\hat{\boldsymbol{e}}_{\parallel}$, which originate from the wave splitting dyadic $\mathbf{W}$, that assures that the correct radiation in the upper half space is fulfilled. The branch points contributes to the field as a lateral or head wave, but do not contribute to the radiated power [9, 15]. The transverse electric field in the spatial domain is (similar expression for the other fields), see (2.2)

$$\begin{aligned}\boldsymbol{E}_{xy}(\boldsymbol{r}) =& \frac{1}{4\pi^2}\iint_{-\infty}^{\infty} \boldsymbol{E}_{xy}(\boldsymbol{k}_t, z)e^{\mathrm{i}\boldsymbol{k}_t\cdot\boldsymbol{\rho}}\,\mathrm{d}k_x\,\mathrm{d}k_y \\ =& \frac{1}{4\pi^2}\int_0^{\infty} k_t\,\mathrm{d}k_t \int_0^{2\pi} \mathrm{d}\alpha \boldsymbol{E}_{xy}(k_t,\alpha,z)e^{\mathrm{i}k_t\rho\cos(\alpha-\phi)}\end{aligned} \tag{6.1}$$

where $\rho = \sqrt{x^2+y^2}$ is the lateral distance to the origin and ϕ is the azimuth angle in the x-y-plane.

Inside the substrate, $0 \le z < d$, the spectral field quantities are, see (3.4) and (3.5)

$$\begin{cases} \boldsymbol{E}_{xy}(\boldsymbol{k}_t, z) = -\mathbf{P}_{12}(\boldsymbol{k}_t, z, 0)\cdot\mathbf{D}(\boldsymbol{k}_t)\cdot\eta_0\boldsymbol{J}_S(\boldsymbol{k}_t) \\ \eta_0\mathbf{J}\cdot\boldsymbol{H}_{xy}(\boldsymbol{k}_t, z) = -\mathbf{P}_{22}(\boldsymbol{k}_t, z, 0)\cdot\mathbf{D}(\boldsymbol{k}_t)\cdot\eta_0\boldsymbol{J}_S(\boldsymbol{k}_t) \end{cases} \tag{6.2}$$

where

$$\mathbf{D}(\boldsymbol{k}_t) = \left(\mathbf{P}_{22}(\boldsymbol{k}_t, d, 0) + \mathbf{W}^{-1}(\boldsymbol{k}_t)\cdot\mathbf{P}_{12}(\boldsymbol{k}_t, d, 0)\right)^{-1}$$

Similarly, for $z > d$, we have, see (3.6) and (3.7)

$$\begin{cases} \boldsymbol{E}_{xy}(\boldsymbol{k}_t, z) = -\mathbf{P}_{12}(\boldsymbol{k}_t, d, 0)\cdot\mathbf{D}(\boldsymbol{k}_t)\cdot\eta_0\boldsymbol{J}_S(\boldsymbol{k}_t)\mathrm{e}^{\mathrm{i}k_z(z-d)} \\ \eta_0\mathbf{J}\cdot\boldsymbol{H}_{xy}(\boldsymbol{k}_t, z) = \mathbf{W}^{-1}(\boldsymbol{k}_t)\cdot\mathbf{P}_{12}(\boldsymbol{k}_t, d, 0)\cdot\mathbf{D}(\boldsymbol{k}_t)\cdot\eta_0\boldsymbol{J}_S(\boldsymbol{k}_t)\mathrm{e}^{\mathrm{i}k_z(z-d)} \end{cases} \tag{6.3}$$

From the knowledge of the transverse components of the electric and the magnetic field, the z-components of the fields are then easily found, see (2.6)

$$\begin{cases} E_z(\boldsymbol{k}_t, z) = \dfrac{\eta_0}{k_0\epsilon(z)}\boldsymbol{k}_t\cdot\mathbf{J}\cdot\boldsymbol{H}_{xy}(\boldsymbol{k}_t, z) \\ \eta_0 H_z(\boldsymbol{k}_t, z) = -\dfrac{1}{k_0\mu(z)}\boldsymbol{k}_t\cdot\mathbf{J}\cdot\boldsymbol{E}_{xy}(\boldsymbol{k}_t, z) \end{cases} \tag{6.4}$$

The power radiated by the surface wave is obtained from the Poynting vector integrated over a cylindrical surface (evaluated as $\rho \to \infty$). The explicit expression is

$$P_{\mathrm{sw}} = \frac{1}{2}\,\mathrm{Re}\int_0^{\infty}\mathrm{d}z\int_0^{2\pi}\mathrm{d}\phi\;\rho\hat{\boldsymbol{\rho}}\cdot(\boldsymbol{E}_{\mathrm{sw}}(\boldsymbol{r})\times\boldsymbol{H}^*_{\mathrm{sw}}(\boldsymbol{r})) \tag{6.5}$$

where the fields $\boldsymbol{E}_{\mathrm{sw}}$ and $\boldsymbol{H}_{\mathrm{sw}}$ are the electric and the magnetic fields, respectively, of the surface wave, which are found below.

Using the expressions of the spectral domain fields above, this expression can be rewritten as

$$P_{\rm sw} = \frac{1}{32\pi^4}\,{\rm Re}\int_0^\infty {\rm d}z \int_0^{2\pi} {\rm d}\phi \times \iint_{-\infty}^{\infty} {\rm d}\boldsymbol{k}_t \iint_{-\infty}^{\infty} {\rm d}\boldsymbol{k}_t'\; \rho\hat{\boldsymbol{\rho}}\cdot(\boldsymbol{E}_{\rm sw}(\boldsymbol{k}_t,z)\times\boldsymbol{H}_{\rm sw}^*(\boldsymbol{k}_t',z))\, e^{{\rm i}(\boldsymbol{k}_t-\boldsymbol{k}_t')\cdot\boldsymbol{\rho}}$$

The radiation efficiency e is then defined as the quotient between the power radiated into the half space, $P_{\rm r}$, and the total power radiated $P_{\rm r}+P_{\rm sw}$, *i.e.*,

$$e = \frac{P_{\rm r}}{P_{\rm r}+P_{\rm sw}} \tag{6.6}$$

where $P_{\rm r}$ is given by (5.4) and $P_{\rm sw}$ by (6.5).

6.1 The TM-case (circular patch)

We assume that only one surface mode contributes in the calculations below. This is the case for sufficiently low frequencies at which only the $\rm TM_0$-mode, which has zero cut-off frequency, is excited. Moreover, we let the patch be a circular patch of radius a. The current on the circular patch is given in Section 5.2, see (5.2). In this case the fields in the substrate can be found by the calculus of residues.

For a circular patch, the electric and the magnetic fields in the substrate ($0 \le z < d$) are, see (6.2), (6.4), (2.16), and (5.2)

$$\begin{cases} \boldsymbol{E}_{xy}^{\rm TM}(\boldsymbol{k}_t,z) = -\dfrac{k_z P_{12}^{\rm TM}(k_t,z,0)}{k_z P_{22}^{\rm TM}(k_t,d,0)+k_0 P_{12}^{\rm TM}(k_t,d,0)}\eta_0 J_S^{\rm TM}(k_t)\cos\alpha\hat{\boldsymbol{e}}_\parallel \\ \eta_0\mathbf{J}\cdot\boldsymbol{H}_{xy}^{\rm TM}(\boldsymbol{k}_t,z) = -\dfrac{k_z P_{22}^{\rm TM}(k_t,z,0)}{k_z P_{22}^{\rm TM}(k_t,d,0)+k_0 P_{12}^{\rm TM}(k_t,d,0)}\eta_0 J_S^{\rm TM}(k_t)\cos\alpha\hat{\boldsymbol{e}}_\parallel \\ E_z^{\rm TM}(\boldsymbol{k}_t,z) = -\dfrac{k_t}{k_0\epsilon(z)}\dfrac{k_z P_{22}^{\rm TM}(k_t,z,0)}{k_z P_{22}^{\rm TM}(k_t,d,0)+k_0 P_{12}^{\rm TM}(k_t,d,0)}\eta_0 J_S^{\rm TM}(k_t)\cos\alpha \\ \eta_0 H_z^{\rm TM}(\boldsymbol{k}_t,z) = 0 \end{cases}$$

where

$$J_S^{\rm TM}(k_t) = \frac{4\pi a^2\eta_{11}J_1(\eta_{11})J_1'(k_t a)}{\eta_{11}^2-k_t^2a^2}$$

Similarly for $z > d$ (vacuum), we get, see (6.3) and (6.4)

$$\begin{cases} \boldsymbol{E}_{xy}^{\rm TM}(\boldsymbol{k}_t,z) = -\dfrac{k_z P_{12}^{\rm TM}(k_t,d,0)}{k_z P_{22}^{\rm TM}(k_t,d,0)+k_0 P_{12}^{\rm TM}(k_t,d,0)}\eta_0 J_S^{\rm TM}(k_t){\rm e}^{{\rm i}k_z(z-d)}\cos\alpha\hat{\boldsymbol{e}}_\parallel \\ \eta_0\mathbf{J}\cdot\boldsymbol{H}_{xy}^{\rm TM}(\boldsymbol{k}_t,z) = \dfrac{k_0 P_{12}^{\rm TM}(k_t,d,0)}{k_z P_{22}^{\rm TM}(k_t,d,0)+k_0 P_{12}^{\rm TM}(k_t,d,0)}\eta_0 J_S^{\rm TM}(k_t){\rm e}^{{\rm i}k_z(z-d)}\cos\alpha\hat{\boldsymbol{e}}_\parallel \\ E_z^{\rm TM}(\boldsymbol{k}_t,z) = \dfrac{k_t P_{12}^{\rm TM}(k_t,d,0)}{k_z P_{22}^{\rm TM}(k_t,d,0)+k_0 P_{12}^{\rm TM}(k_t,d,0)}\eta_0 J_S^{\rm TM}(k_t){\rm e}^{{\rm i}k_z(z-d)}\cos\alpha \\ \eta_0 H_z^{\rm TM}(\boldsymbol{k}_t,z) = 0 \end{cases}$$

Evaluation of the α integral in (6.1) gives ($0 \le z < d$)

$$\begin{cases} \hat{\boldsymbol{\rho}} \cdot \boldsymbol{E}_{xy}(\boldsymbol{r}) = -\dfrac{\cos\phi}{2\pi} \displaystyle\int_0^\infty k_t \ \mathrm{d}k_t F^{\mathrm{TM}}(k_t, z) J_1'(k_t\rho) \\ \hat{\boldsymbol{\phi}} \cdot \boldsymbol{E}_{xy}(\boldsymbol{r}) = \dfrac{\sin\phi}{2\pi} \displaystyle\int_0^\infty k_t \ \mathrm{d}k_t F^{\mathrm{TM}}(k_t, z) \dfrac{J_1(k_t\rho)}{k_t\rho} \\ E_z(\boldsymbol{r}) = -\mathrm{i}\dfrac{\cos\phi}{2\pi} \displaystyle\int_0^\infty k_t \ \mathrm{d}k_t \dfrac{k_t}{k_0\epsilon(z)} G^{\mathrm{TM}}(k_t, z) J_1(k_t\rho) \\ \eta_0 \hat{\boldsymbol{\rho}} \cdot \boldsymbol{H}_{xy}(\boldsymbol{r}) = \dfrac{\sin\phi}{2\pi} \displaystyle\int_0^\infty k_t \ \mathrm{d}k_t G^{\mathrm{TM}}(k_t, z) \dfrac{J_1(k_t\rho)}{k_t\rho} \\ \eta_0 \hat{\boldsymbol{\phi}} \cdot \boldsymbol{H}_{xy}(\boldsymbol{r}) = \dfrac{\cos\phi}{2\pi} \displaystyle\int_0^\infty k_t \ \mathrm{d}k_t G^{\mathrm{TM}}(k_t, z) J_1'(k_t\rho) \end{cases}$$

where we have adopted the following notion for the common parts of the integrands:

$$\begin{cases} F^{\mathrm{TM}}(k_t, z) = \dfrac{k_z P_{12}^{\mathrm{TM}}(k_t, z, 0)}{k_z P_{22}^{\mathrm{TM}}(k_t, d, 0) + k_0 P_{12}^{\mathrm{TM}}(k_t, d, 0)} \eta_0 J_S^{\mathrm{TM}}(k_t) \\ G^{\mathrm{TM}}(k_t, z) = \dfrac{k_z P_{22}^{\mathrm{TM}}(k_t, z, 0)}{k_z P_{22}^{\mathrm{TM}}(k_t, d, 0) + k_0 P_{12}^{\mathrm{TM}}(k_t, d, 0)} \eta_0 J_S^{\mathrm{TM}}(k_t) \end{cases} \tag{6.7}$$

These results are obtained by the use of the following integrals:

$$\int_0^{2\pi} e^{\mathrm{i}k_t\rho\cos(\phi-\alpha)} \begin{pmatrix} \cos m\phi \\ \sin m\phi \end{pmatrix} \mathrm{d}\,\phi = 2\pi \mathrm{i}^m J_m(k_t\rho) \begin{pmatrix} \cos m\alpha \\ \sin m\alpha \end{pmatrix}$$

and

$$\begin{aligned} \int_0^{2\pi} e^{\mathrm{i}k_t\rho\cos(\alpha-\phi)} \begin{pmatrix} \cos m\alpha \\ \sin m\alpha \end{pmatrix} \hat{\boldsymbol{e}}_\parallel \ \mathrm{d}\,\alpha &= \frac{2\pi\mathrm{i}^{m-1}}{k_t} \nabla J_m(k_t\rho) \begin{pmatrix} \cos m\phi \\ \sin m\phi \end{pmatrix} \\ &= 2\pi\mathrm{i}^{m-1} \left(\hat{\boldsymbol{\rho}} J_m'(k_t\rho) \begin{pmatrix} \cos m\phi \\ \sin m\phi \end{pmatrix} + \hat{\boldsymbol{\phi}} \frac{m J_m(k_t\rho)}{k_t\rho} \begin{pmatrix} -\sin m\phi \\ \cos m\phi \end{pmatrix} \right) \end{aligned}$$

Similarly the contributions for $z > d$ (vacuum) are

$$\begin{cases} \hat{\boldsymbol{\rho}} \cdot \boldsymbol{E}_{xy}(\boldsymbol{r}) = -\dfrac{\cos\phi}{2\pi} \displaystyle\int_0^\infty k_t \ \mathrm{d}k_t F^{\mathrm{TM}}(k_t, d) J_1'(k_t\rho) \mathrm{e}^{\mathrm{i}k_z(z-d)} \\ \hat{\boldsymbol{\phi}} \cdot \boldsymbol{E}_{xy}(\boldsymbol{r}) = \dfrac{\sin\phi}{2\pi} \displaystyle\int_0^\infty k_t \ \mathrm{d}k_t F^{\mathrm{TM}}(k_t, d) \dfrac{J_1(k_t\rho)}{k_t\rho} \mathrm{e}^{\mathrm{i}k_z(z-d)} \\ E_z(\boldsymbol{r}) = \mathrm{i}\dfrac{\cos\phi}{2\pi} \displaystyle\int_0^\infty k_t \ \mathrm{d}k_t \dfrac{k_t}{k_z} F^{\mathrm{TM}}(k_t, d) J_1(k_t\rho) \mathrm{e}^{\mathrm{i}k_z(z-d)} \\ \eta_0 \hat{\boldsymbol{\rho}} \cdot \boldsymbol{H}_{xy}(\boldsymbol{r}) = -\dfrac{\sin\phi}{2\pi} \displaystyle\int_0^\infty k_t \ \mathrm{d}k_t \dfrac{k_0}{k_z} F^{\mathrm{TM}}(k_t, d) \dfrac{J_1(k_t\rho)}{k_t\rho} \mathrm{e}^{\mathrm{i}k_z(z-d)} \\ \eta_0 \hat{\boldsymbol{\phi}} \cdot \boldsymbol{H}_{xy}(\boldsymbol{r}) = -\dfrac{\cos\phi}{2\pi} \displaystyle\int_0^\infty k_t \ \mathrm{d}k_t \dfrac{k_0}{k_z} F^{\mathrm{TM}}(k_t, d) J_1'(k_t\rho) \mathrm{e}^{\mathrm{i}k_z(z-d)} \end{cases}$$

These integrals can be rewritten in a more symmetric form, which facilitates the

evaluation of the integral for large values of ρ. The result is $(0 \leq z < d)$

$$\begin{cases} \hat{\boldsymbol{\rho}} \cdot \boldsymbol{E}_{xy}(\boldsymbol{r}) = -\dfrac{\cos\phi}{4\pi} \displaystyle\int_{-\infty}^{\infty} k_t \ \mathrm{d}k_t F^{\mathrm{TM}}(k_t, z) H_1^{(1)\prime}(k_t\rho) \\ \hat{\boldsymbol{\phi}} \cdot \boldsymbol{E}_{xy}(\boldsymbol{r}) = \dfrac{\sin\phi}{4\pi} \displaystyle\int_{-\infty}^{\infty} k_t \ \mathrm{d}k_t F^{\mathrm{TM}}(k_t, z) \dfrac{H_1^{(1)}(k_t\rho)}{k_t\rho} \\ E_z(\boldsymbol{r}) = -\mathrm{i}\dfrac{\cos\phi}{4\pi} \displaystyle\int_{-\infty}^{\infty} k_t \ \mathrm{d}k_t \dfrac{k_t}{k_0\epsilon(z)} G^{\mathrm{TM}}(k_t, z) H_1^{(1)}(k_t\rho) \\ \eta_0\hat{\boldsymbol{\rho}} \cdot \boldsymbol{H}_{xy}(\boldsymbol{r}) = \dfrac{\sin\phi}{4\pi} \displaystyle\int_{-\infty}^{\infty} k_t \ \mathrm{d}k_t G^{\mathrm{TM}}(k_t, z) \dfrac{H_1^{(1)}(k_t\rho)}{k_t\rho} \\ \eta_0\hat{\boldsymbol{\phi}} \cdot \boldsymbol{H}_{xy}(\boldsymbol{r}) = \dfrac{\cos\phi}{4\pi} \displaystyle\int_{-\infty}^{\infty} k_t \ \mathrm{d}k_t G^{\mathrm{TM}}(k_t, z) H_1^{(1)\prime}(k_t\rho) \end{cases}$$

and for $z > d$ (vacuum)

$$\begin{cases} \hat{\boldsymbol{\rho}} \cdot \boldsymbol{E}_{xy}(\boldsymbol{r}) = -\dfrac{\cos\phi}{4\pi} \displaystyle\int_{-\infty}^{\infty} k_t \ \mathrm{d}k_t F^{\mathrm{TM}}(k_t, d) H_1^{(1)\prime}(k_t\rho) \mathrm{e}^{\mathrm{i}k_z(z-d)} \\ \hat{\boldsymbol{\phi}} \cdot \boldsymbol{E}_{xy}(\boldsymbol{r}) = \dfrac{\sin\phi}{4\pi} \displaystyle\int_{-\infty}^{\infty} k_t \ \mathrm{d}k_t F^{\mathrm{TM}}(k_t, d) \dfrac{H_1^{(1)}(k_t\rho)}{k_t\rho} \mathrm{e}^{\mathrm{i}k_z(z-d)} \\ E_z(\boldsymbol{r}) = \mathrm{i}\dfrac{\cos\phi}{4\pi} \displaystyle\int_{-\infty}^{\infty} k_t \ \mathrm{d}k_t \dfrac{k_t}{k_z} F^{\mathrm{TM}}(k_t, d) H_1^{(1)}(k_t\rho) \mathrm{e}^{\mathrm{i}k_z(z-d)} \\ \eta_0\hat{\boldsymbol{\rho}} \cdot \boldsymbol{H}_{xy}(\boldsymbol{r}) = -\dfrac{\sin\phi}{4\pi} \displaystyle\int_{-\infty}^{\infty} k_t \ \mathrm{d}k_t \dfrac{k_0}{k_z} F^{\mathrm{TM}}(k_t, d) \dfrac{H_1^{(1)}(k_t\rho)}{k_t\rho} \mathrm{e}^{\mathrm{i}k_z(z-d)} \\ \eta_0\hat{\boldsymbol{\phi}} \cdot \boldsymbol{H}_{xy}(\boldsymbol{r}) = -\dfrac{\cos\phi}{4\pi} \displaystyle\int_{-\infty}^{\infty} k_t \ \mathrm{d}k_t \dfrac{k_0}{k_z} F^{\mathrm{TM}}(k_t, d) H_1^{(1)\prime}(k_t\rho) \mathrm{e}^{\mathrm{i}k_z(z-d)} \end{cases}$$

where we used the analytic continuation $H_n^{(2)}(ze^{-\mathrm{i}\pi}) = -e^{\mathrm{i}n\pi} H_n^{(1)}(z)$ of the Hankel functions, and the fact that the rest of the integrand is an odd function of k_t. The integration contour along the real axis follows the negative real k_t-axis above the branch line of the Hankel function from the origin along the negative real axis, and continuous below the positive real k_t-axis [15].

6.1.1 Surface mode fields

Until now the general expressions of the fields have been given. We are now interested in the dominant contribution of these fields at a large (lateral) distance from the patch, *i.e.*, $\rho \to \infty$. The pole at the surface mode $\boldsymbol{k}_{t\mathrm{sw}} = k_{t\mathrm{sw}}\hat{\boldsymbol{e}}_{\parallel}$ gives the lowest order contribution to the fields [15, Ch. 4, Sec. 5.6]. We assume that this pole is a real number located on the positive axis and that $k_{t\mathrm{sw}} > k_0$. This corresponds to the case of a lossless material in the substrate. A lossy substrate shows a surface wave contribution with an exponentially deceasing amplitude in the lateral directions and this case is of no interest in this context.

Calculus of residues gives us the components that contribute to the radiated power (the $\hat{\boldsymbol{\phi}}$- and the $\hat{\boldsymbol{z}}$-components) in the substrate, $(0 \leq z < d)$ (dominant

contribution as $\rho \to \infty$). The result is

$$\begin{cases} E_z(\boldsymbol{r}) = \dfrac{\cos\phi}{2} \dfrac{k_{t_{\rm sw}}^2}{k_0 \epsilon(z)} \operatorname{Res} G^{\rm TM}(k_{t_{\rm sw}}, z) \sqrt{\dfrac{2}{\pi k_{t_{\rm sw}} \rho}} e^{{\rm i}(k_{t_{\rm sw}}\rho - 3\pi/4)} \\ \eta_0 \hat{\boldsymbol{\phi}} \cdot \boldsymbol{H}_{xy}(\boldsymbol{r}) = {\rm i} \dfrac{\cos\phi}{2} k_{t_{\rm sw}} \operatorname{Res} G^{\rm TM}(k_{t_{\rm sw}}, z) \sqrt{\dfrac{2}{\pi k_{t_{\rm sw}} \rho}} e^{{\rm i}(k_{t_{\rm sw}}\rho - \pi/4)} \end{cases}$$

where the residues of the functions $F^{\rm TM}$ and $G^{\rm TM}$ defined in (6.7) are denoted $\operatorname{Res} F^{\rm TM}$ and $\operatorname{Res} G^{\rm TM}$. For a homogeneous, isotropic material these residues are found explicitly, see Appendix F. In the inhomogeneous case they are solutions of a system of ODEs, see Section 6.2. Note that

$$E_z(\boldsymbol{r}) = -\eta_0 \hat{\boldsymbol{\phi}} \cdot \boldsymbol{H}_{xy}(\boldsymbol{r}) \frac{k_{t_{\rm sw}}}{k_0 \epsilon(z)}, \qquad 0 \le z < d$$

All other components either do not contribute to the power of the surface mode, or vanish faster than $\rho^{-1/2}$ as $\rho \to \infty$.

Similarly, above the patch in vacuum ($z > d$) we get a similar result

$$\begin{cases} E_z(\boldsymbol{r}) = -\dfrac{\cos\phi}{2} \dfrac{k_{t_{\rm sw}}^2}{{\rm i}\sqrt{k_{t_{\rm sw}}^2 - k_0^2}} \operatorname{Res} F^{\rm TM}(k_{t_{\rm sw}}, d) \\ \qquad \sqrt{\dfrac{2}{\pi k_{t_{\rm sw}} \rho}} e^{{\rm i}(k_{t_{\rm sw}}\rho - 3\pi/4)} {\rm e}^{-\sqrt{k_{t_{\rm sw}}^2 - k_0^2}(z-d)} \\ \eta_0 \hat{\boldsymbol{\phi}} \cdot \boldsymbol{H}_{xy}(\boldsymbol{r}) = -\dfrac{\cos\phi}{2} \dfrac{k_0 k_{t_{\rm sw}}}{\sqrt{k_{t_{\rm sw}}^2 - k_0^2}} \operatorname{Res} F^{\rm TM}(k_{t_{\rm sw}}, d) \\ \qquad \sqrt{\dfrac{2}{\pi k_{t_{\rm sw}} \rho}} e^{{\rm i}(k_{t_{\rm sw}}\rho - \pi/4)} {\rm e}^{-\sqrt{k_{t_{\rm sw}}^2 - k_0^2}(z-d)} \end{cases}$$

Note that

$$E_z(\boldsymbol{r}) = -\eta_0 \hat{\boldsymbol{\phi}} \cdot \boldsymbol{H}_{xy}(\boldsymbol{r}) \frac{k_{t_{\rm sw}}}{k_0}, \qquad z > d$$

In Figure 12, we depict the vertical electrical field, E_z, inside and outside the substrate for permittivity profiles 1) and 2) in (4.3). The thickness of the substrate is $d = 0.1\lambda_0$. The vertical electric field is normalized with the value of the field at the top of the substrate, and we can only make conclusions about the relative distribution of the field inside and outside the substrate. We see that the increasing permittivity profile shows larger variation in the vertical electric field in the substrate compared to the decreasing permittivity profile.

Finally, we write down the expression of the power radiated by the surface wave,

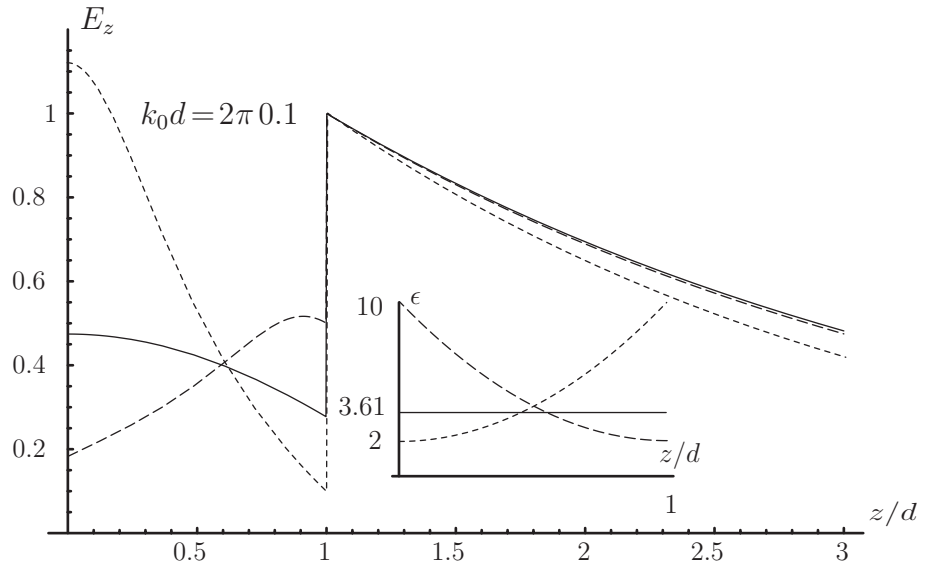

Figure 12: The vertical electrical field, E_z, inside and outside the substrate for the permittivity profiles 1) (dotted line) and 2) (dashed line) in (4.3) as a function of the variable z/d. The thickness of the substrate is $d = 0.1\lambda_0$. The solid line is the field for the homogenized permittivity profile. The vertical electric field is normalized with the value of the field at the top of the substrate.

(6.5). The result is ($k_{t\mathrm{sw}}$ and $\epsilon(z)$ are assumed real)

$$
\begin{aligned}
P_{\mathrm{sw}} =& \frac{1}{\pi\eta_0}\frac{1}{4}\int_0^d \mathrm{d}z \int_0^{2\pi} \mathrm{d}\phi \frac{k_{t\mathrm{sw}}^2 \cos^2\phi}{k_0\epsilon(z)} \left|\mathrm{Res}\, G^{\mathrm{TM}}(k_{t\mathrm{sw}}, z)\right|^2 \\
&+ \frac{1}{\pi\eta_0}\frac{1}{4}\int_d^\infty \mathrm{d}z \int_0^{2\pi} \mathrm{d}\phi \frac{k_0 k_{t\mathrm{sw}}^2 \cos^2\phi}{k_{t\mathrm{sw}}^2 - k_0^2} \left|\mathrm{Res}\, F^{\mathrm{TM}}(k_{t\mathrm{sw}}, d)\right|^2 \mathrm{e}^{-2\sqrt{k_{t\mathrm{sw}}^2 - k_0^2}(z-d)} \\
=& \frac{k_{t\mathrm{sw}}^2}{4\eta_0 k_0}\int_0^d \frac{1}{\epsilon(z)} \left|\mathrm{Res}\, G^{\mathrm{TM}}(k_{t\mathrm{sw}}, z)\right|^2 \mathrm{d}z + \frac{k_0 k_{t\mathrm{sw}}^2}{8\eta_0\left(k_{t\mathrm{sw}}^2 - k_0^2\right)^{3/2}} \left|\mathrm{Res}\, F^{\mathrm{TM}}(k_{t\mathrm{sw}}, d)\right|^2
\end{aligned}
$$

From the equations above, one derives the leading behavior of the power radiated by the surface wave in terms of the parameter $k_0 d$. The integral term contributes as $O((k_0 d)^5)$, and the second term contributes as $O((k_0 d)^3)$. The overall behavior therefore is $P_{\mathrm{sw}} = O((k_0 d)^3)$.

6.2 Surface mode — residues

The residues of the quantities $F^{\mathrm{TM}}(k_t, z)$ and $G^{\mathrm{TM}}(k_t, z)$, defined in (6.7), must be known to continue the calculations of the surface wave power. In the inhomogeneous substrate case these residues must be computed numerically. In this section, we

derive a set of ODEs, which solution gives the desired result. The residues for a homogeneous substrate are calculated explicitly, see Appendix F.

The starting point for a calculation of the residues in the isotropic TM-case is, see (2.11).

$$\begin{cases} \dfrac{\mathrm{d}}{\mathrm{d}z}P_{12}^{\mathrm{TM}} = \mathrm{i}k_0\left(\dfrac{k_t^2}{k_0^2\epsilon(z)} - \mu(z)\right)P_{22}^{\mathrm{TM}} \\ \dfrac{\mathrm{d}}{\mathrm{d}z}P_{22}^{\mathrm{TM}} = -\mathrm{i}k_0\epsilon(z)P_{12}^{\mathrm{TM}} \end{cases} \qquad \begin{cases} P_{12}^{\mathrm{TM}}(k_t,0,0) = 0 \\ P_{22}^{\mathrm{TM}}(k_t,0,0) = 1 \end{cases}$$

We introduce a new dependent variable $D(\boldsymbol{k}_t, z)$ defined as

$$D(k_t, z) = k_z P_{22}^{\mathrm{TM}}(k_t, z, 0) + k_0 P_{12}^{\mathrm{TM}}(k_t, z, 0)$$

From the ODE of P_{12}^{TM} and P_{22}^{TM}, D and P_{12}^{TM} satisfy the following system of ODEs:

$$\begin{cases} \dfrac{\mathrm{d}}{\mathrm{d}z}D = -\mathrm{i}k_0k_z\epsilon(z)P_{12}^{\mathrm{TM}} + \mathrm{i}\dfrac{k_0^2}{k_z}\left(\dfrac{k_t^2}{k_0^2\epsilon(z)} - \mu(z)\right)\left(D - k_0P_{12}^{\mathrm{TM}}\right) \\ \dfrac{\mathrm{d}}{\mathrm{d}z}P_{12}^{\mathrm{TM}} = \mathrm{i}\dfrac{k_0}{k_z}\left(\dfrac{k_t^2}{k_0^2\epsilon(z)} - \mu(z)\right)\left(D - k_0P_{12}^{\mathrm{TM}}\right) \end{cases}$$

with initial conditions

$$\begin{cases} D(k_t, 0) = k_z \\ P_{12}^{\mathrm{TM}}(k_t, 0, 0) = 0 \end{cases}$$

To proceed, differentiate these equations w.r.t. k_t and we get (prime denotes derivative w.r.t. k_t).

$$\begin{cases} \dfrac{\mathrm{d}}{\mathrm{d}z}D' = -\mathrm{i}k_0k_z\epsilon(z)\left(P_{12}^{\mathrm{TM}}\right)' + \mathrm{i}\dfrac{k_0^2}{k_z}\left(\dfrac{k_t^2}{k_0^2\epsilon(z)} - \mu(z)\right)\left(D' - k_0\left(P_{12}^{\mathrm{TM}}\right)'\right) \\ \qquad\qquad + \mathrm{i}\dfrac{k_0k_t}{k_z}\epsilon(z)P_{12}^{\mathrm{TM}} + \mathrm{i}\dfrac{k_0^2k_t}{k_z^2}\left(\dfrac{k_t^2}{k_0^2\epsilon(z)} - \mu(z)\right)P_{22}^{\mathrm{TM}} + \mathrm{i}\dfrac{2k_t}{\epsilon(z)}P_{22}^{\mathrm{TM}} \\ \dfrac{\mathrm{d}}{\mathrm{d}z}\left(P_{12}^{\mathrm{TM}}\right)' = \mathrm{i}\dfrac{k_0}{k_z}\left(\dfrac{k_t^2}{k_0^2\epsilon(z)} - \mu(z)\right)\left(D' - k_0\left(P_{12}^{\mathrm{TM}}\right)'\right) \\ \qquad\qquad + \mathrm{i}\dfrac{k_0k_t}{k_z^2}\left(\dfrac{k_t^2}{k_0^2\epsilon(z)} - \mu(z)\right)P_{22}^{\mathrm{TM}} + \mathrm{i}\dfrac{2k_t}{k_0\epsilon(z)}P_{22}^{\mathrm{TM}} \end{cases}$$

with initial conditions

$$\begin{cases} D'(k_t, 0) = -k_t/k_z \\ \left(P_{12}^{\mathrm{TM}}\right)'(k_t, 0, 0) = 0 \end{cases}$$

Note that the functions D and $\left(P_{12}^{\mathrm{TM}}\right)'$ are odd functions in the variable k_t and they are analytic functions of k_t except for a branch point at $k_t = k_0$ [43]. Note also that the propagators P_{12}^{TM} and P_{22}^{TM} act as source terms in these equations. The solution to this set of ODEs gives us the residues $F^{\mathrm{TM}}(k_t, z)$ and $G^{\mathrm{TM}}(k_t, z)$ as

$$\operatorname{Res} F^{\mathrm{TM}}(k_{t\mathrm{sw}}, z) = \frac{k_z|_{k_{t\mathrm{sw}}}\, P_{12}^{\mathrm{TM}}(k_{t\mathrm{sw}}, z, 0)}{D'(k_{t\mathrm{sw}}, d)}\eta_0 J_S^{\mathrm{TM}}(k_{t\mathrm{sw}})$$

$$\operatorname{Res} G^{\mathrm{TM}}(k_{t\mathrm{sw}}, z) = \frac{k_z|_{k_{t\mathrm{sw}}}\, P_{22}^{\mathrm{TM}}(k_{t\mathrm{sw}}, z, 0)}{D'(k_{t\mathrm{sw}}, d)}\eta_0 J_S^{\mathrm{TM}}(k_{t\mathrm{sw}})$$

The exact values of these residues for a homogenous substrate are found in Appendix F. An asymptotic analysis of these ODEs as $k_0 d \to 0$ gives the asymptotic behavior of the residues above as $k_0 d \to 0$. The result is

$$\operatorname{Res} F^{\mathrm{TM}}(k_{t\mathrm{sw}}, z) = \frac{\mathrm{i}k_0^3 d^3 \left(\epsilon_h \mu_h - 1\right)^2 \eta_0 J_S^{\mathrm{TM}}(k_0)}{\epsilon_h^2} \int_0^{z/d} \left[\frac{1}{\epsilon(td)} - \mu(td)\right] \mathrm{d}t + O\left((k_0 d)^5\right)$$

$$\operatorname{Res} G^{\mathrm{TM}}(k_{t\mathrm{sw}}, z) = \frac{k_0^2 d^2 \left(\epsilon_h \mu_h - 1\right)^2 \eta_0 J_S^{\mathrm{TM}}(k_0)}{\epsilon_h^2} + O\left((k_0 d)^4\right)$$

where the homogenized values of the relative permittivity, ϵ_h, and the relative permeability, μ_h, are given in (2.13).

6.3 Numerical examples

This section contains a series of numerical simulations for typical substrate profiles below a circular parch antenna. The definition of the profiles used in the simulations is specified in Section 4.2, see (4.3). The relation between the radius a of the patch and the resonance frequency is approximated by (5.3), *i.e.*,

$$k_0 a = \frac{1.841}{\sqrt{\epsilon_h \mu_h}} \tag{6.8}$$

where the homogenized (vertical) values of the relative permittivity and the relative permeability, ϵ_h and μ_h, respectively, are defined in (2.13).

The first example is a computation of the radiation efficiency, defined in (6.6), for a circular patch antenna. Figure 13 shows the radiation efficiency (in dB) for a series of profiles (decreasing and increasing quadratic and reciprocal profiles) as a function of the substrate thickness normalized by the radius of the patch, *i.e.*, d/a. We observe that the radiation efficiency has the limit 1 (0 dB) as the thickness of the substrate vanishes. This effect is due to fact that $P_{\mathrm{r}} = O((k_0 d)^2)$ and $P_{\mathrm{sw}} = O((k_0 d)^3)$ in the limit of vanishing thickness $k_0 d$. We also notice an increased radiation efficiency in the increasing profile cases, profiles 1) and 6), compared with the decreasing profiles 3) and 7). Moreover, the figure shows that the lower the permittivity the higher radiation efficiency, even though the homogenized permittivities are the same for the profiles 6) and 7).

Figure 14 illustrates the small thickness behavior from a different viewpoint. The figure depicts the radiation efficiency for permittivity profile 7) and its homogenized profile. We see that the two curves are identical for small thicknesses, and, therefore, the inhomogeneous substrate behaves as a homogenized profile for small substrate thicknesses. The differences between the radiation characteristics are also shown in Figure 15 which shows the quantity $P_{\mathrm{r}}/P_{\mathrm{sw}}$ (in dB) as a function of d/a.

In Figure 16 the directivity of the profiles in Figures 13 and 15 are presented. The directivity is normalized with the radiation intensity from the antenna in the vertical direction averaged over all directions. As for the radiation efficiency, there is a significant difference in directivity between the different permittivity profiles. Again,

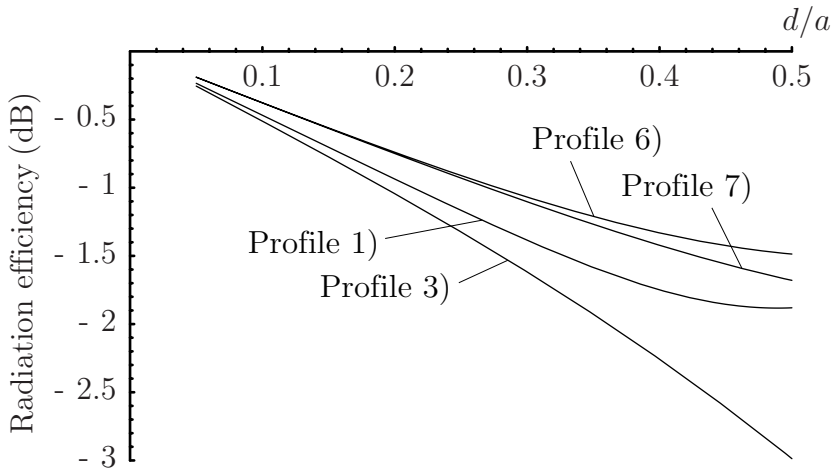

Figure 13: The radiation efficiency (in dB) for four different permittivity profiles as a function of d/a. The permittivity profiles are profile 1), 3), 6), and 7) defined in (4.3).

the increasing profiles, profiles 1) and 6), give a higher directivity, and the lower the permittivity, profiles 6) and 7), the higher the directivity. For small substrate thickness, the directivity approaches different values depending on the homogenized permittivity profile value. This is seen more clearly from Figure 17, where we clearly see that the small thickness behavior is determined by the homogenized substrate profile. Note that different permittivity profiles imply different values of $k_0 a$, see (6.8), and, therefore, different directivity.

7 Conclusions

The numerical computations presented in this paper show that the radiation efficiency and the directivity of the patch antenna depend strongly on the electric properties of the substrate. Specifically, an increasing permittivity profile gives higher radiation efficiency and directivity than the corresponding decreasing one (the profile turned upside down). The small thickness behavior of both the radiation efficiency and the directivity is determined by the homogenized values of the electric parameters of the substrate.

The analysis presented in this paper has several generalizations, some of which are rather obvious or trivial. There are no difficulties in generalizing the analysis to the case of an anisotropic or, more generally, a bianisotropic substrate. Moreover, it is straightforward to add a superstrate on top of the patch as well as additional patches. The resonance frequencies and the bandwidth computations require a full Method of Moment implementation. These extensions will be addressed in a future paper.

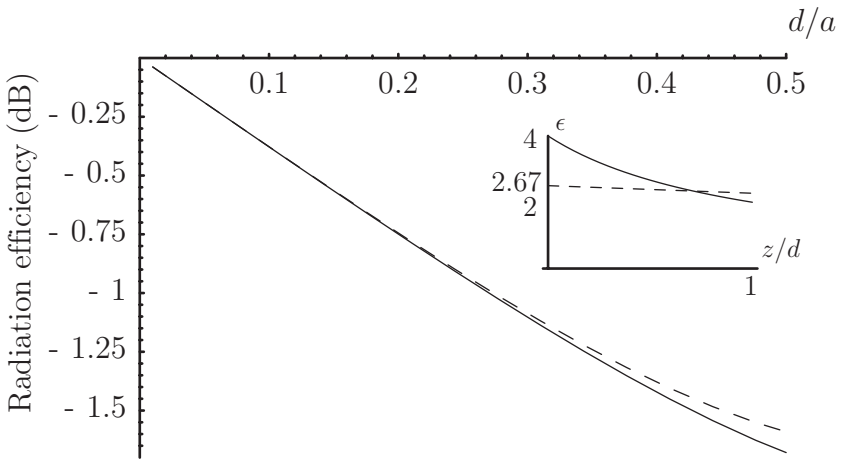

Figure 14: The radiation efficiency (in dB) for permittivity profile 7) defined in (4.3), as a function of d/a. The solid line shows the radiation efficiency for the inhomogeneous profile, and the dashed line depicts the radiation efficiency for the homogenized profile.

Acknowledgement

The work reported in this paper is supported by a grant from the Swedish Foundation for Strategic Research (SSF), which is gratefully acknowledged. The authors also like to thank L. Vegni, F. Bilotti, and A. Toscano for useful comments.

Appendix A Dynamics

In this appendix we deduce the fundamental equation for an isotropic media. The fundamental equation is a set of ordinary differential equations (ODEs) in the transverse field components. A more complete derivation of the fundamental equation for a general bianisotropic material is given in [34, 35].

The Maxwell equations for time harmonic fields (the time convention adopted in this paper is $\exp(-\mathrm{i}\omega t)$) for an isotropic media is

$$\begin{cases} \nabla \times \boldsymbol{E}(\boldsymbol{r}) = \mathrm{i}\omega\mu_0\mu(z)\boldsymbol{H}(\boldsymbol{r}) \\ \nabla \times \boldsymbol{H}(\boldsymbol{r}) = \boldsymbol{J}(\boldsymbol{r},t) - \mathrm{i}\omega\epsilon_0\epsilon(z)\boldsymbol{E}(\boldsymbol{r}) \end{cases}$$

where the isotropic material is modelled by the relative permittivity $\epsilon(z)$ and the relative permeability $\mu(z)$, which both can be inhomogeneous w.r.t. the depth coordinate z. The permittivity and permeability of vacuum are denoted by ϵ_0 and μ_0, respectively.

A spatial Fourier transform, (2.1), of the Maxwell equations in x- and y-directions

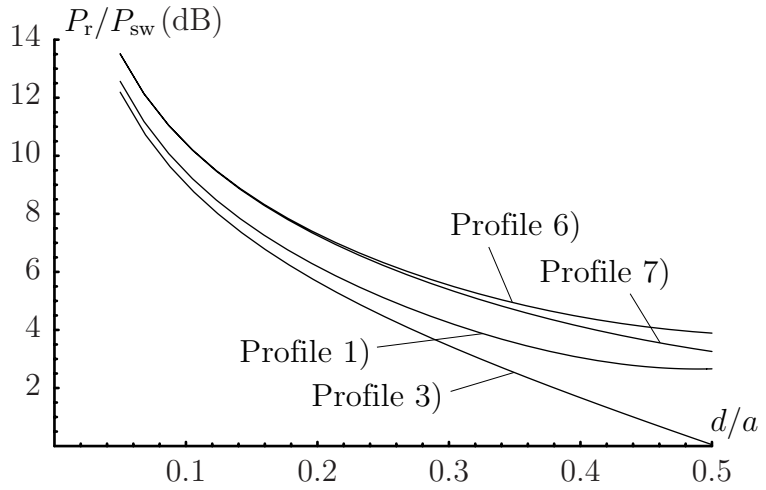

Figure 15: The quotient P_r/P_{sw} (in dB) for four different permittivity profiles as a function of d/a. The permittivity profiles are profile 1), 3), 6), and 7) defined in (4.3).

implies

$$\begin{cases} \dfrac{\mathrm{d}}{\mathrm{d}z}\mathbf{J}\cdot\boldsymbol{E} + \mathrm{i}\boldsymbol{k}_t\times\boldsymbol{E} = \mathrm{i}\omega\mu_0\mu\boldsymbol{H} \\ \dfrac{\mathrm{d}}{\mathrm{d}z}\mathbf{J}\cdot\boldsymbol{H} + \mathrm{i}\boldsymbol{k}_t\times\boldsymbol{H} = -\mathrm{i}\omega\epsilon_0\epsilon\boldsymbol{E} + \boldsymbol{J} \end{cases} \tag{A.1}$$

where[4] $\mathbf{J}\cdot\boldsymbol{A} = \hat{\boldsymbol{z}}\times\boldsymbol{A}$ denotes a rotation of $\pi/2$ in the x-y-plane and $\mathbf{J}\cdot\mathbf{J} = -\mathbf{I}_2$. The argument in all fields $\boldsymbol{E}$, $\boldsymbol{H}$ and $\boldsymbol{J}$ is $(\boldsymbol{k}_t, z)$. Scalar multiplication with $-\mathbf{J}$ gives

$$\begin{cases} \dfrac{\mathrm{d}}{\mathrm{d}z}\boldsymbol{E}_{xy} - \mathrm{i}\mathbf{J}\cdot(\boldsymbol{k}_t\times\boldsymbol{E}) = -\mathrm{i}\omega\mu_0\mu\mathbf{J}\cdot\boldsymbol{H} \\ \dfrac{\mathrm{d}}{\mathrm{d}z}\mathbf{J}\cdot\boldsymbol{H} + \mathrm{i}\boldsymbol{k}_t\times\boldsymbol{H} = -\mathrm{i}\omega\epsilon_0\epsilon\boldsymbol{E} + \boldsymbol{J} \end{cases}$$

The following vector identities are used for simplifications of the equations:

$$\begin{cases} \mathbf{J}\cdot(\boldsymbol{k}_t\times\boldsymbol{E}) = \hat{\boldsymbol{z}}\times(\boldsymbol{k}_t\times\boldsymbol{E}) = \boldsymbol{k}_t(\hat{\boldsymbol{z}}\cdot\boldsymbol{E}) - \boldsymbol{E}\underbrace{(\hat{\boldsymbol{z}}\cdot\boldsymbol{k}_t)}_{=0} = \boldsymbol{k}_t E_z \\ \boldsymbol{k}_t\times\boldsymbol{H} = \boldsymbol{k}_t\times\boldsymbol{H}_{xy} + \boldsymbol{k}_t\times\hat{\boldsymbol{z}}H_z = \boldsymbol{k}_t\times\boldsymbol{H}_{xy} - \mathbf{J}\cdot\boldsymbol{k}_t H_z \end{cases}$$

and we get by projection of the x-y-components

$$\begin{cases} \dfrac{\mathrm{d}}{\mathrm{d}z}\boldsymbol{E}_{xy} - \mathrm{i}\boldsymbol{k}_t E_z = -\mathrm{i}\omega\mu_0\mu\mathbf{J}\cdot\boldsymbol{H}_{xy} \\ \dfrac{\mathrm{d}}{\mathrm{d}z}\mathbf{J}\cdot\boldsymbol{H}_{xy} - \mathrm{i}\mathbf{J}\cdot\boldsymbol{k}_t H_z = -\mathrm{i}\omega\epsilon_0\epsilon\boldsymbol{E}_{xy} + \boldsymbol{J}_{xy} \end{cases} \tag{A.2}$$

[4]Note the typographical difference between the dyadic $\mathbf{J}$ which denotes a rotation, and the current density vector $\boldsymbol{J}$. All vectors in this paper are typed in italic bold face and dyadics are printed in roman bold face. The identity dyadic in n dimensions is denoted $\mathbf{I}_n$.

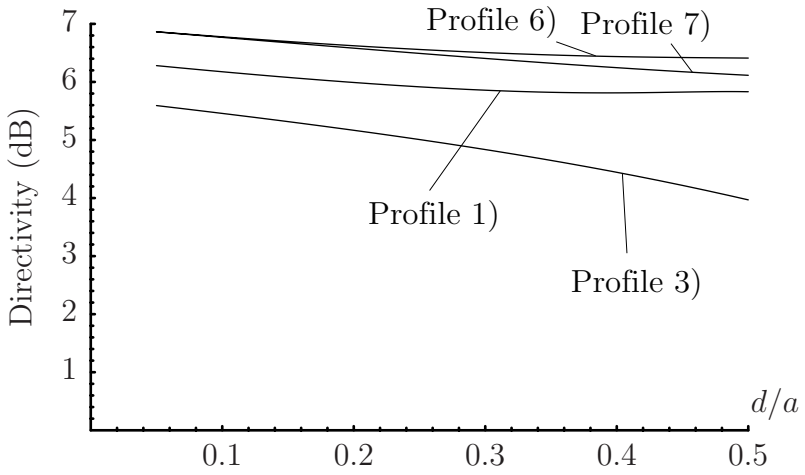

Figure 16: The directivity for the four different permittivity profiles 1), 3), 6), and 7) defined in (4.3), as a function of d/a. The directivity is normalized with an isotropic radiation over the whole space.

The z-components are most conveniently obtained by a scalar multiplication with $\hat{\boldsymbol{z}}$ in (A.1). The result is

$$\begin{cases} -\boldsymbol{k}_t \cdot \mathbf{J} \cdot \boldsymbol{E}_{xy} = \omega\mu_0\mu H_z \\ -\mathrm{i}\boldsymbol{k}_t \cdot (\mathbf{J} \cdot \boldsymbol{H}_{xy}) = -\mathrm{i}\omega\epsilon_0\epsilon E_z + J_z \end{cases} \tag{A.3}$$

If E_z and H_z are eliminated from equation (A.2) we get

$$\begin{cases} \dfrac{\mathrm{d}}{\mathrm{d}z}\boldsymbol{E}_{xy} = \left(\mathrm{i}\dfrac{\boldsymbol{k}_t\boldsymbol{k}_t}{\omega\epsilon_0\epsilon} - \mathrm{i}\omega\mu_0\mu\mathbf{I}_2\right) \cdot \mathbf{J} \cdot \boldsymbol{H}_{xy} + \dfrac{\boldsymbol{k}_t J_z}{\omega\epsilon_0\epsilon} \\ \dfrac{\mathrm{d}}{\mathrm{d}z}\mathbf{J} \cdot \boldsymbol{H}_{xy} = \left(-\mathrm{i}\dfrac{\mathbf{J} \cdot \boldsymbol{k}_t\boldsymbol{k}_t \cdot \mathbf{J}}{\omega\mu_0\mu} - \mathrm{i}\omega\epsilon_0\epsilon\mathbf{I}_2\right) \cdot \boldsymbol{E}_{xy} + \boldsymbol{J}_{xy} \end{cases}$$

This is the fundamental equation and we write it in its canonical form as

$$\begin{aligned} \frac{\mathrm{d}}{\mathrm{d}z}\begin{pmatrix} \boldsymbol{E}_{xy}(z) \\ \eta_0\mathbf{J} \cdot \boldsymbol{H}_{xy}(z) \end{pmatrix} =& \mathrm{i}k_0 \begin{pmatrix} \mathbf{M}_{11}(z) & \mathbf{M}_{12}(z) \\ \mathbf{M}_{21}(z) & \mathbf{M}_{22}(z) \end{pmatrix} \cdot \begin{pmatrix} \boldsymbol{E}_{xy}(z) \\ \eta_0\mathbf{J} \cdot \boldsymbol{H}_{xy}(z) \end{pmatrix} \\ &+ \eta_0 \begin{pmatrix} \boldsymbol{k}_t J_z(z)/\left(k_0\epsilon(z)\right) \\ \boldsymbol{J}_{xy}(z) \end{pmatrix} \\ =& \mathrm{i}k_0\mathbf{M}(z) \cdot \begin{pmatrix} \boldsymbol{E}_{xy}(z) \\ \eta_0\mathbf{J} \cdot \boldsymbol{H}_{xy}(z) \end{pmatrix} + \eta_0 \begin{pmatrix} \boldsymbol{k}_t J_z(z)/\left(k_0\epsilon(z)\right) \\ \boldsymbol{J}_{xy}(z) \end{pmatrix} \end{aligned} \tag{A.4}$$

where

$$\begin{cases} \mathbf{M}_{11} = \mathbf{M}_{22} = \mathbf{0} \\ \mathbf{M}_{12} = \dfrac{\boldsymbol{k}_t\boldsymbol{k}_t}{k_0\eta_0\omega\epsilon_0\epsilon} - \dfrac{\omega\mu_0\mu}{\eta_0 k_0}\mathbf{I}_2 = -\mu\mathbf{I}_2 + \dfrac{\boldsymbol{k}_t\boldsymbol{k}_t}{k_0^2\epsilon} \\ \mathbf{M}_{21} = -\eta_0\dfrac{\mathbf{J} \cdot \boldsymbol{k}_t\boldsymbol{k}_t \cdot \mathbf{J}}{k_0\omega\mu_0\mu} - \dfrac{\eta_0\omega\epsilon_0\epsilon}{k_0}\mathbf{I}_2 = -\epsilon\mathbf{I}_2 - \dfrac{1}{\mu k_0^2}\mathbf{J} \cdot \boldsymbol{k}_t\boldsymbol{k}_t \cdot \mathbf{J} \end{cases} \tag{A.5}$$

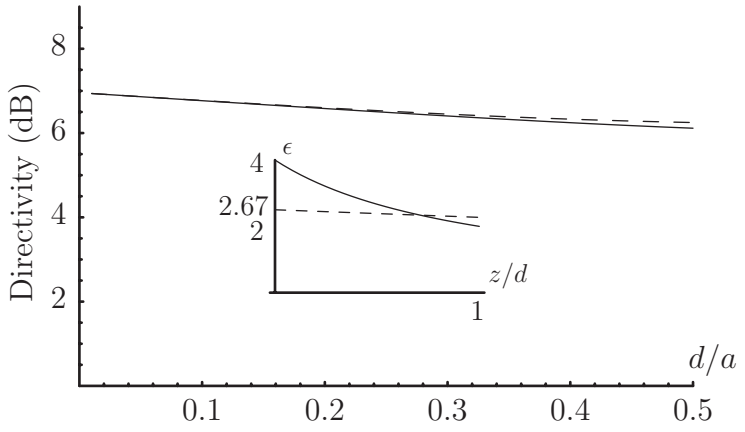

Figure 17: The directivity for permittivity profile 7) defined in (4.3), as a function of d/a. The solid line shows the directivity for the inhomogeneous profile, and the dashed line depicts the directivity for the homogenized profile.

The argument in the dyadics $\mathbf{M}_{ij}$, $i,j = 1,2$ is $(\boldsymbol{k}_t, z)$. One advantage with this first order formulation is that no differentiation of the material parameters ϵ and μ is needed. If we try to eliminate one of the field components, differentiation of the material parameters becomes necessary.

From the knowledge of the tangential fields, we obtain the z-components from (A.3). In the absence of J_z, we get

$$\begin{cases} E_z = \dfrac{\eta_0}{k_0\epsilon}\boldsymbol{k}_t \cdot \mathbf{J} \cdot \boldsymbol{H}_{xy} \\ \eta_0 H_z = -\dfrac{1}{k_0\mu}\boldsymbol{k}_t \cdot \mathbf{J} \cdot \boldsymbol{E}_{xy} \end{cases} \tag{A.6}$$

Appendix B Wave splitting

The wave splitting transformation was introduced in Section 2.3. This transformation makes it easy to verify that the fields in the half space satisfy the correct radiation conditions. In this wave splitting transformation, the transverse $\boldsymbol{E}$ and $\boldsymbol{H}$ fields are transformed into two other fields, one field, $\boldsymbol{F}^+$, moving in the upwards z-direction and one in the opposite direction, $\boldsymbol{F}^-$. The splitting in vacuum is given by [30, 35]

$$\begin{pmatrix} \boldsymbol{F}^+(\boldsymbol{k}_t, z) \\ \boldsymbol{F}^-(\boldsymbol{k}_t, z) \end{pmatrix} = \frac{1}{2}\begin{pmatrix} \mathbf{I}_2 & -\mathbf{W}(\boldsymbol{k}_t) \\ \mathbf{I}_2 & \mathbf{W}(\boldsymbol{k}_t) \end{pmatrix} \cdot \begin{pmatrix} \boldsymbol{E}_{xy}(\boldsymbol{k}_t, z) \\ \eta_0 \mathbf{J} \cdot \boldsymbol{H}_{xy}(\boldsymbol{k}_t, z) \end{pmatrix}$$

The splitting dyadic $\mathbf{W}$ and its inverse are defined by

$$\begin{cases} \mathbf{W}(\boldsymbol{k}_t) = \dfrac{k_z}{k_0}\left(\mathbf{I}_2 - \dfrac{1}{k_z^2}\boldsymbol{k}_t \times (\boldsymbol{k}_t \times \mathbf{I}_2)\right) = \dfrac{k_z}{k_0}\hat{\boldsymbol{e}}_\parallel\hat{\boldsymbol{e}}_\parallel + \dfrac{k_0}{k_z}\hat{\boldsymbol{e}}_\perp\hat{\boldsymbol{e}}_\perp \\ \mathbf{W}^{-1}(\boldsymbol{k}_t) = \dfrac{k_0}{k_z}\left(\mathbf{I}_2 + \dfrac{1}{k_0^2}\boldsymbol{k}_t \times (\boldsymbol{k}_t \times \mathbf{I}_2)\right) = \dfrac{k_0}{k_z}\hat{\boldsymbol{e}}_\parallel\hat{\boldsymbol{e}}_\parallel + \dfrac{k_z}{k_0}\hat{\boldsymbol{e}}_\perp\hat{\boldsymbol{e}}_\perp \end{cases}$$

If we combine the wave splitting above with (A.4) we get

$$\begin{aligned}\frac{\mathrm{d}}{\mathrm{d}z}\begin{pmatrix}\boldsymbol{F}^+\\ \boldsymbol{F}^-\end{pmatrix} &= \frac{1}{2}\begin{pmatrix}\mathbf{I}_2 & -\mathbf{W}\\ \mathbf{I}_2 & \mathbf{W}\end{pmatrix}\cdot\frac{\mathrm{d}}{\mathrm{d}z}\begin{pmatrix}\boldsymbol{E}_{xy}\\ \eta_0\mathbf{J}\cdot\boldsymbol{H}_{xy}\end{pmatrix}\\ &= \frac{1}{2}\begin{pmatrix}\mathbf{I}_2 & -\mathbf{W}\\ \mathbf{I}_2 & \mathbf{W}\end{pmatrix}\cdot\left[\mathrm{i}k_0\begin{pmatrix}\mathbf{M}_{11} & \mathbf{M}_{12}\\ \mathbf{M}_{21} & \mathbf{M}_{22}\end{pmatrix}\cdot\begin{pmatrix}\boldsymbol{E}_{xy}\\ \eta_0\mathbf{J}\cdot\boldsymbol{H}_{xy}\end{pmatrix}+\eta_0\begin{pmatrix}\boldsymbol{k}_t J_z/\left(k_0\epsilon\right)\\ \boldsymbol{J}_{xy}\end{pmatrix}\right]\end{aligned}$$

If we also use the inverse splitting transformation, see (2.17)

$$\begin{pmatrix}\boldsymbol{E}_{xy}\\ \eta_0\mathbf{J}\cdot\boldsymbol{H}_{xy}\end{pmatrix} = \begin{pmatrix}\mathbf{I}_2 & \mathbf{I}_2\\ -\mathbf{W}^{-1} & \mathbf{W}^{-1}\end{pmatrix}\cdot\begin{pmatrix}\boldsymbol{F}^+\\ \boldsymbol{F}^-\end{pmatrix}$$

we get

$$\begin{aligned}\frac{\mathrm{d}}{\mathrm{d}z}\begin{pmatrix}\boldsymbol{F}^+\\ \boldsymbol{F}^-\end{pmatrix} &= \frac{\mathrm{i}k_0}{2}\begin{pmatrix}-\mathbf{W}\cdot\mathbf{M}_{21}-\mathbf{M}_{12}\cdot\mathbf{W}^{-1} & -\mathbf{W}\cdot\mathbf{M}_{21}+\mathbf{M}_{12}\cdot\mathbf{W}^{-1}\\ \mathbf{W}\cdot\mathbf{M}_{21}-\mathbf{M}_{12}\cdot\mathbf{W}^{-1} & \mathbf{W}\cdot\mathbf{M}_{21}+\mathbf{M}_{12}\cdot\mathbf{W}^{-1}\end{pmatrix}\cdot\begin{pmatrix}\boldsymbol{F}^+\\ \boldsymbol{F}^-\end{pmatrix}\\ &+\frac{\eta_0}{2}\begin{pmatrix}\boldsymbol{k}_t J_z/\left(k_0\epsilon\right)-\mathbf{W}\cdot\boldsymbol{J}_{xy}\\ \boldsymbol{k}_t J_z/\left(k_0\epsilon\right)+\mathbf{W}\cdot\boldsymbol{J}_{xy}\end{pmatrix}\end{aligned} \tag{B.1}$$

In a vacuous region, $\mu=\epsilon=1$, we can simplify these equations further. In vacuum the non-zero parts of the matrices $\mathbf{M}_{ij}$, $i,j=1,2$, are

$$\begin{cases}\mathbf{M}_{12} = -\mathbf{I}_2+\dfrac{\boldsymbol{k}_t\boldsymbol{k}_t}{k_0^2}\\ \mathbf{M}_{21} = -\mathbf{I}_2-\dfrac{\mathbf{J}\cdot\boldsymbol{k}_t\boldsymbol{k}_t\cdot\mathbf{J}}{k_0^2}\end{cases} \tag{B.2}$$

Moreover, some useful vector and dyadic identities are

$$\mathbf{I}_2 = \frac{\boldsymbol{k}_t\boldsymbol{k}_t}{k_t^2}-\frac{\mathbf{J}\cdot\boldsymbol{k}_t\boldsymbol{k}_t\cdot\mathbf{J}}{k_t^2} \tag{B.3}$$

$$\boldsymbol{k}_t\times\left(\boldsymbol{k}_t\times\mathbf{I}_2\right) = \mathbf{J}\cdot\boldsymbol{k}_t\boldsymbol{k}_t\cdot\mathbf{J} \tag{B.4}$$

$$k_0^2 = k_t^2+k_z^2 \tag{B.5}$$

$$\boldsymbol{k}_t\times\left(\boldsymbol{k}_t\times\mathbf{I}_2\right)\cdot\mathbf{J}\cdot\boldsymbol{k}_t = -k_t^2\mathbf{J}\cdot\boldsymbol{k}_t \tag{B.6}$$

$$\boldsymbol{k}_t\boldsymbol{k}_t\cdot\left[\boldsymbol{k}_t\times\left(\boldsymbol{k}_t\times\mathbf{I}_2\right)\right] = \mathbf{0} \tag{B.7}$$

We get

$$\begin{aligned}\mathbf{W}\cdot\mathbf{M}_{21}\pm\mathbf{M}_{12}\cdot\mathbf{W}^{-1} =& \frac{k_z}{k_0}\left(\mathbf{I}_2-\frac{1}{k_z^2}\boldsymbol{k}_t\times\left(\boldsymbol{k}_t\times\mathbf{I}_2\right)\right)\cdot\left(-\mathbf{I}_2-\frac{\mathbf{J}\cdot\boldsymbol{k}_t\boldsymbol{k}_t\cdot\mathbf{J}}{k_0^2}\right)\\ &\pm\frac{k_0}{k_z}\left(-\mathbf{I}_2+\frac{\boldsymbol{k}_t\boldsymbol{k}_t}{k_0^2}\right)\cdot\left(\mathbf{I}_2+\frac{1}{k_0^2}\boldsymbol{k}_t\times\left(\boldsymbol{k}_t\times\mathbf{I}_2\right)\right)\end{aligned}$$

Using (B.4), (B.6) and (B.7) we can simplify this expression.

$$\begin{aligned}\mathbf{W}\cdot\mathbf{M}_{21}\pm\mathbf{M}_{12}\cdot\mathbf{W}^{-1} =& \mathbf{J}\cdot\boldsymbol{k}_t\boldsymbol{k}_t\cdot\mathbf{J}\left(-\frac{k_z}{k_0^3}+\frac{1}{k_0k_z}-\frac{k_t^2}{k_0^3k_z}\mp\frac{1}{k_0k_z}\right)\\ &-\frac{k_z}{k_0}\mathbf{I}_2\mp\frac{k_0}{k_z}\mathbf{I}_2\pm\frac{\boldsymbol{k}_t\boldsymbol{k}_t}{k_zk_0}\end{aligned}$$

Equation (B.5) simplifies it further

$$\mathbf{W}\cdot\mathbf{M}_{21}\pm\mathbf{M}_{12}\cdot\mathbf{W}^{-1}=\frac{1}{k_0k_z}\left(\mp\mathbf{J}\cdot\boldsymbol{k}_t\boldsymbol{k}_t\cdot\mathbf{J}-k_z^2\mathbf{I}_2\mp k_0^2\mathbf{I}_2\pm\boldsymbol{k}_t\boldsymbol{k}_t\right)$$

and together with (B.3) and (B.5) we get

$$\mathbf{W}\cdot\mathbf{M}_{21}\pm\mathbf{M}_{12}\cdot\mathbf{W}^{-1}=\frac{k_z}{k_0}(-1\mp1)\mathbf{I}_2$$

The final expression for the dynamics, in vacuum, becomes

$$\frac{\mathrm{d}}{\mathrm{d}z}\begin{pmatrix}\boldsymbol{F}^+\\ \boldsymbol{F}^-\end{pmatrix}=\mathrm{i}\begin{pmatrix}k_z\mathbf{I}_2 & \mathbf{0}\\ \mathbf{0} & -k_z\mathbf{I}_2\end{pmatrix}\cdot\begin{pmatrix}\boldsymbol{F}^+\\ \boldsymbol{F}^-\end{pmatrix}+\frac{\eta_0}{2}\begin{pmatrix}\boldsymbol{k}_tJ_z/k_0-\mathbf{W}\cdot\boldsymbol{J}_{xy}\\ \boldsymbol{k}_tJ_z/k_0+\mathbf{W}\cdot\boldsymbol{J}_{xy}\end{pmatrix}\tag{B.8}$$

Appendix C Alternative solution to the radiation problem

Here, we derive an alternative, more traditional, solution of the radiation in the half space. The reflection dyadic, $\mathbf{r}(\boldsymbol{k}_t)$, of the substrate is used instead of the propagators. The wave splitting analysis in Section 2.3 and Appendix B is, however, used in this appendix.

For a stratified, bianisotropic slab the reflection dyadic is readily found by 4×4 matrix algebra. This technique is presented in detail in [35], and here we present the results of this analysis. An alternative way of finding the reflection dyadic is to employ an imbedding technique, which leads to the Riccati equation. This technique is presented in Section C.1.

Above the patch, we apply the radiation condition, $\boldsymbol{F}^-(z>d)=\mathbf{0}$, and by (2.17) we have

$$\begin{pmatrix}\boldsymbol{E}_{xy}(\boldsymbol{k}_t,z)\\ \eta_0\mathbf{J}\cdot\boldsymbol{H}_{xy}(\boldsymbol{k}_t,z)\end{pmatrix}=\begin{pmatrix}\boldsymbol{F}^+(\boldsymbol{k}_t,z)\\ -\mathbf{W}^{-1}(\boldsymbol{k}_t)\cdot\boldsymbol{F}^+(\boldsymbol{k}_t,z)\end{pmatrix}\qquad z>d\tag{C.1}$$

The solutions to the split fields in vacuum are, see (2.20)

$$\boldsymbol{F}^\pm(\boldsymbol{k}_t,z)=\mathrm{e}^{\pm\mathrm{i}k_z(z-d)}\boldsymbol{F}^\pm(\boldsymbol{k}_t,d^+),\qquad z>d$$

Just below the patch, $z=d^-$, we have the traditional linear relation between the upgoing and downgoing parts of the electric field in terms of the reflection dyadic, $\mathbf{r}(\boldsymbol{k}_t)$, of the substrate, *i.e.*,

$$\boldsymbol{F}^+(z=d^-)=\mathbf{r}\cdot\boldsymbol{F}^-(z=d^-)\tag{C.2}$$

By the use of (2.17) we get

$$\begin{pmatrix}\boldsymbol{E}_{xy}(\boldsymbol{k}_t,d^-)\\ \eta_0\mathbf{J}\cdot\boldsymbol{H}_{xy}(\boldsymbol{k}_t,d^-)\end{pmatrix}=\begin{pmatrix}(\mathbf{I}_2+\mathbf{r}(\boldsymbol{k}_t))\cdot\boldsymbol{F}^-(\boldsymbol{k}_t,d^-)\\ \mathbf{W}^{-1}(\boldsymbol{k}_t)\cdot(\mathbf{I}_2-\mathbf{r}(\boldsymbol{k}_t))\cdot\boldsymbol{F}^-(\boldsymbol{k}_t,d^-)\end{pmatrix}\tag{C.3}$$

Subtract the fields on both sides of the patch, *i.e.*, equation (C.1) evaluated at $z = d^+$ and (C.3), and use the boundary conditions on the patch. We get

$$\begin{pmatrix} \mathbf{0} \\ \eta_0 \boldsymbol{J}_S(\boldsymbol{k}_t) \end{pmatrix} = \begin{pmatrix} \boldsymbol{F}^+(\boldsymbol{k}_t, d^+) - (\mathbf{I}_2 + \mathbf{r}(\boldsymbol{k}_t)) \cdot \boldsymbol{F}^-(\boldsymbol{k}_t, d^-) \\ -\mathbf{W}^{-1}(\boldsymbol{k}_t) \cdot \boldsymbol{F}^+(\boldsymbol{k}_t, d^+) - \mathbf{W}^{-1}(\boldsymbol{k}_t) \cdot (\mathbf{I}_2 - \mathbf{r}(\boldsymbol{k}_t)) \cdot \boldsymbol{F}^-(\boldsymbol{k}_t, d^-) \end{pmatrix}$$

where the total surface current density on the patch is denoted

$$\boldsymbol{J}_S(\boldsymbol{k}_t) = \mathbf{J} \cdot \boldsymbol{H}_{xy}(\boldsymbol{k}_t, d^+) - \mathbf{J} \cdot \boldsymbol{H}_{xy}(\boldsymbol{k}_t, d^-)$$

Solve for the fields $\eta_0 \boldsymbol{J}_S(\boldsymbol{k}_t)$ and $\boldsymbol{F}^+(\boldsymbol{k}_t, d^+)$. The result is

$$\begin{cases} \eta_0 \boldsymbol{J}_S(\boldsymbol{k}_t) = -2\mathbf{W}^{-1}(\boldsymbol{k}_t) \cdot \boldsymbol{F}^-(\boldsymbol{k}_t, d^-) \\ \boldsymbol{F}^+(\boldsymbol{k}_t, d^+) = (\mathbf{I}_2 + \mathbf{r}(\boldsymbol{k}_t)) \cdot \boldsymbol{F}^-(\boldsymbol{k}_t, d^-) \end{cases}$$

For $z > d$ we get

$$\boldsymbol{F}^+(\boldsymbol{k}_t, z) = -\frac{\eta_0}{2} \mathrm{e}^{\mathrm{i}k_z(z-d)} \left(\mathbf{W}(\boldsymbol{k}_t) + \mathbf{r}(\boldsymbol{k}_t) \cdot \mathbf{W}(\boldsymbol{k}_t)\right) \cdot \boldsymbol{J}_S(\boldsymbol{k}_t) \tag{C.4}$$

which is another way of expressing the solution in the half space in terms of the total surface current density on the patch.

The reflection dyadic is the unknown quantity in the approach adopted in this appendix. One very efficient way of computing this dyadic is presented in [35]. The rest of this appendix is devoted to an alternative way of finding the refection dyadic of the substrate as the solution to a system of non-linear ODEs.

C.1 The Riccati equation

In this section we exploit the dynamics in $0 < z < d$, see, *e.g.*, (2.18) (source-free region)

$$\frac{\mathrm{d}}{\mathrm{d}z} \begin{pmatrix} \boldsymbol{F}^+ \\ \boldsymbol{F}^- \end{pmatrix} = \frac{\mathrm{i}k_0}{2} \begin{pmatrix} \mathbf{U}_{11} & \mathbf{U}_{12} \\ \mathbf{U}_{21} & \mathbf{U}_{22} \end{pmatrix} \cdot \begin{pmatrix} \boldsymbol{F}^+ \\ \boldsymbol{F}^- \end{pmatrix} \tag{C.5}$$

where the dyadics $\mathbf{U}_{11}$, $\mathbf{U}_{12}$, $\mathbf{U}_{21}$, and $\mathbf{U}_{22}$ are given in (2.19). For an isotropic material, we explicitly have

$$\begin{cases} \mathbf{U}_{11} = -\mathbf{U}_{22} = \dfrac{k_z}{k_0} \left\{ \left(\epsilon + \dfrac{k_0^2}{k_z^2}\mu - \dfrac{k_t^2}{\epsilon k_z^2} \right) \hat{\boldsymbol{e}}_\parallel \hat{\boldsymbol{e}}_\parallel + \left(\mu + \dfrac{k_0^2}{k_z^2}\epsilon - \dfrac{k_t^2}{\mu k_z^2} \right) \hat{\boldsymbol{e}}_\perp \hat{\boldsymbol{e}}_\perp \right\} \\ \mathbf{U}_{12} = -\mathbf{U}_{21} = \dfrac{k_z}{k_0} \left\{ \left(\epsilon - \dfrac{k_0^2}{k_z^2}\mu + \dfrac{k_t^2}{\epsilon k_z^2} \right) \hat{\boldsymbol{e}}_\parallel \hat{\boldsymbol{e}}_\parallel + \left(-\mu + \dfrac{k_0^2}{k_z^2}\epsilon - \dfrac{k_t^2}{\mu k_z^2} \right) \hat{\boldsymbol{e}}_\perp \hat{\boldsymbol{e}}_\perp \right\} \end{cases} \tag{C.6}$$

The final goal is to find the reflection dyadic, $\mathbf{r}$, of the substrate filling the space between $z = 0$ and $z = d$. This dyadic gives the linear relation between the up- and down-going parts of the field, *i.e.*,

$$\boldsymbol{F}^+(d) = \mathbf{r} \cdot \boldsymbol{F}^-(d)$$

To solve this problem, we formulate a more general reflection problem for a subsection $[0, z]$ of the entire slab $[0, d]$. The relation between the fields $\boldsymbol{F}^+(z)$ and $\boldsymbol{F}^-(z)$ is linear, and the mapping $\mathbf{r}(z)$ is defined by

$$\boldsymbol{F}^+(z) = \mathbf{r}(z) \cdot \boldsymbol{F}^-(z), \qquad 0 < z < d \tag{C.7}$$

The dyadic $\mathbf{r}(z)$ is the reflection dyadic for a truncated subproblem in which the material only fills the space between $z = 0$ and z. If we can find how the dyadic $\mathbf{r}(z)$ changes with a change in z, we can find the sought reflection dyadic of the entire substrate as the solution $\mathbf{r} = \mathbf{r}(d)$. This procedure of finding the reflection dyadic is also called an imbedding procedure [4, 17].

In order to find this imbedding relation, first differentiate the right hand side of (C.7) w.r.t. z and use (C.5) and (C.7).

$$\begin{aligned}
\frac{\mathrm{d}}{\mathrm{d}z}(\mathbf{r}(z) \cdot \boldsymbol{F}^-(z)) &= \frac{\mathrm{d}\mathbf{r}(z)}{\mathrm{d}z} \cdot \boldsymbol{F}^-(z) + \mathbf{r}(z) \cdot \frac{\mathrm{d}\boldsymbol{F}^-(z)}{\mathrm{d}z} \\
&= \frac{\mathrm{d}\mathbf{r}(z)}{\mathrm{d}z} \cdot \boldsymbol{F}^-(z) + \mathbf{r}(z) \cdot \frac{\mathrm{i}k_0}{2} \left(\mathbf{U}_{21} \cdot \boldsymbol{F}^+(z) + \mathbf{U}_{22} \cdot \boldsymbol{F}^-(z) \right) \\
&= \frac{\mathrm{d}\mathbf{r}(z)}{\mathrm{d}z} \cdot \boldsymbol{F}^-(z) + \mathbf{r}(z) \cdot \frac{\mathrm{i}k_0}{2} \left(\mathbf{U}_{21} \cdot \mathbf{r}(z) \cdot \boldsymbol{F}^-(z) + \mathbf{U}_{22} \cdot \boldsymbol{F}^-(z) \right)
\end{aligned}$$

Proceed by a differentiation of the left hand side of (C.7) w.r.t. z, and use (C.5) and (C.7).

$$\begin{aligned}
\frac{\mathrm{d}}{\mathrm{d}z}\boldsymbol{F}^+(z) &= \frac{\mathrm{i}k_0}{2}\mathbf{U}_{11} \cdot \boldsymbol{F}^+(z) + \frac{\mathrm{i}k_0}{2}\mathbf{U}_{12} \cdot \boldsymbol{F}^-(z) \\
&= \frac{\mathrm{i}k_0}{2}\mathbf{U}_{11} \cdot \mathbf{r}(z) \cdot \boldsymbol{F}^-(z) + \frac{\mathrm{i}k_0}{2}\mathbf{U}_{12} \cdot \boldsymbol{F}^-(z)
\end{aligned}$$

The two expressions must be identical, and we get, since the field $\boldsymbol{F}^-(z)$ is arbitrary, a system of Riccati equations.

$$\frac{\mathrm{d}\mathbf{r}(z)}{\mathrm{d}z} + \frac{\mathrm{i}k_0}{2} \left(\mathbf{r}(z) \cdot \mathbf{U}_{21}(z) \cdot \mathbf{r}(z) + \mathbf{r}(z) \cdot \mathbf{U}_{22}(z) - \mathbf{U}_{11}(z) \cdot \mathbf{r}(z) \right) = \frac{\mathrm{i}k_0}{2}\mathbf{U}_{12}(z) \tag{C.8}$$

The obvious boundary condition to this ODE is

$$\mathbf{r}(z = 0) = -\mathbf{I}_2$$

since at $z = 0$ the perfectly conducting plane implies $\boldsymbol{F}^+(z = 0) + \boldsymbol{F}^-(z = 0) = \mathbf{0}$.

Appendix D Alternative analysis of the surface waves

In Section 4, we concluded that the surface waves also could be characterized as the $\boldsymbol{k}_t$-values that give zero eigenvalues of the inverse of the reflection dyadic of the slab, *i.e.*, $\mathbf{r}^{-1}$. This observation motivates us to find efficient ways of calculating the dyadic $\mathbf{r}^{-1}$. Two ways are presented in this appendix.

D.1 Riccati equation

The Riccati equation method is very similar to the method of finding $\mathbf{r}$ as a boundary case of a subproblem as presented in Section C.1.

We use the definition of the inverse of the reflection dyadic (subproblem dyadics) $\mathbf{r}(z) \cdot \mathbf{r}^{-1}(z) = \mathbf{r}^{-1}(z) \cdot \mathbf{r}(z) = \mathbf{I}_2$. Differentiation of this relation w.r.t. z gives

$$\frac{\mathrm{d}}{\mathrm{d}z}\mathbf{r}(z) \cdot \mathbf{r}^{-1}(z) + \mathbf{r}(z) \cdot \frac{\mathrm{d}}{\mathrm{d}z}\mathbf{r}^{-1}(z) = \mathbf{0}$$

from which we conclude

$$\frac{\mathrm{d}}{\mathrm{d}z}\mathbf{r}^{-1}(z) = -\mathbf{r}^{-1}(z) \cdot \frac{\mathrm{d}}{\mathrm{d}z}\mathbf{r}(z) \cdot \mathbf{r}^{-1}(z)$$

Equation (C.8) can now be used to eliminate $\frac{\mathrm{d}}{\mathrm{d}z}\mathbf{r}(z)$. We get

$$\frac{\mathrm{d}}{\mathrm{d}z}\mathbf{r}^{-1}(z) + \frac{\mathrm{i}k_0}{2}\left(\mathbf{r}^{-1} \cdot \mathbf{U}_{12} \cdot \mathbf{r}^{-1} + \mathbf{r}^{-1} \cdot \mathbf{U}_{11} - \mathbf{U}_{22} \cdot \mathbf{r}^{-1}\right) = \frac{\mathrm{i}k_0}{2}\mathbf{U}_{21} \tag{D.1}$$

which form is identical to (C.8) ($\mathbf{U}_{11} \leftrightarrow \mathbf{U}_{22}$ and $\mathbf{U}_{12} \leftrightarrow \mathbf{U}_{21}$). By the use of the boundary condition for $\mathbf{r}(z = 0) = -\mathbf{I}_2$ and the definition $\mathbf{r}(z) \cdot \mathbf{r}^{-1}(z) = \mathbf{r}^{-1}(z) \cdot \mathbf{r}(z) = \mathbf{I}_2$ we get the boundary condition at $z = 0$.

$$\mathbf{r}^{-1}(z = 0) = -\mathbf{I}_2$$

The specific values of $\boldsymbol{k}_t$ for surface waves are then determined as the $\boldsymbol{k}_t$-values for which $\mathbf{r}^{-1}(d)$ has eigenvalue 0.

D.2 Change to linear system

The second method to find the inverse of the reflection dyadic utilizes the results in Section D.1 and the following nonlinear change of dependent variables from $\mathbf{r}^{-1}(z)$ to $\mathbf{u}(z)$ (prime denotes differentiation w.r.t. z):

$$\mathbf{r}^{-1}(z) = \mathbf{a}(z) \cdot \mathbf{u}'(z) \cdot \mathbf{u}^{-1}(z) \tag{D.2}$$

The dyadic $\mathbf{a}(z)$ is specified below. Differentiation w.r.t. z gives

$$\frac{\mathrm{d}}{\mathrm{d}z}\mathbf{r}^{-1} = \mathbf{a}' \cdot \mathbf{u}' \cdot \mathbf{u}^{-1} + \mathbf{a} \cdot \mathbf{u}'' \cdot \mathbf{u}^{-1} - \mathbf{a} \cdot \mathbf{u}' \cdot \mathbf{u}^{-1} \cdot \mathbf{u}' \cdot \mathbf{u}^{-1}$$

From (D.1) we can eliminate $\frac{\mathrm{d}}{\mathrm{d}z}\mathbf{r}^{-1}(z)$, and, moreover, if we choose

$$\mathbf{a} = \frac{2}{\mathrm{i}k_0}\mathbf{U}_{12}^{-1}$$

and use of the identity

$$\mathbf{r}^{-1} \cdot \mathbf{U}_{12} \cdot \mathbf{r}^{-1} = \mathbf{a} \cdot \mathbf{u}' \cdot \mathbf{u}^{-1} \cdot \mathbf{U}_{12} \cdot \mathbf{a} \cdot \mathbf{u}' \cdot \mathbf{u}^{-1}$$

we get

$$\frac{2}{\mathrm{i}k_0}\left(\frac{\mathrm{d}}{\mathrm{d}z}\mathbf{U}_{12}^{-1}\right)\cdot\mathbf{u}'\cdot\mathbf{u}^{-1}+\frac{2}{\mathrm{i}k_0}\mathbf{U}_{12}^{-1}\cdot\mathbf{u}''\cdot\mathbf{u}^{-1}$$
$$+\left(\mathbf{U}_{12}^{-1}\cdot\mathbf{u}'\cdot\mathbf{u}^{-1}\cdot\mathbf{U}_{11}-\mathbf{U}_{22}\cdot\mathbf{U}_{12}^{-1}\cdot\mathbf{u}'\cdot\mathbf{u}^{-1}\right)=\frac{\mathrm{i}k_0}{2}\mathbf{U}_{21}$$

or

$$\mathbf{u}''-\left(-\mathbf{U}_{12}'\cdot\mathbf{U}_{12}^{-1}+\frac{\mathrm{i}k_0}{2}\mathbf{U}_{12}\cdot\mathbf{U}_{22}\cdot\mathbf{U}_{12}^{-1}\right)\cdot\mathbf{u}'$$
$$+\frac{\mathrm{i}k_0}{2}\mathbf{u}'\cdot\mathbf{u}^{-1}\cdot\mathbf{U}_{11}\cdot\mathbf{u}+\frac{k_0^2}{4}\mathbf{U}_{12}\cdot\mathbf{U}_{21}\cdot\mathbf{u}=\mathbf{0}$$

For those situations were $\mathbf{U}_{11}$ is a symmetric dyadic, *i.e.*, $\mathbf{U}_{11}\cdot\mathbf{u}=\mathbf{u}\cdot\mathbf{U}_{11}$, we obtain a dramatic simplification and the entire system of equations becomes linear in the unknown $\mathbf{u}$. This is the case of isotropic materials, see (C.6). For these situations, we get

$$\mathbf{u}''-\left(-\mathbf{U}_{12}'\cdot\mathbf{U}_{12}^{-1}+\frac{\mathrm{i}k_0}{2}\mathbf{U}_{12}\cdot\mathbf{U}_{22}\cdot\mathbf{U}_{12}^{-1}+\frac{\mathrm{i}k_0}{2}\mathbf{U}_{11}\right)\cdot\mathbf{u}'+\frac{k_0^2}{4}\mathbf{U}_{12}\cdot\mathbf{U}_{21}\cdot\mathbf{u}=\mathbf{0}$$

which is a second order system of linear ODEs in $\boldsymbol{u}$. The inverse of the reflection dyadic is finally found from the transformation (D.2). Moreover, if $\mathbf{U}_{22}$ is symmetric (as it is for isotropic materials) we get

$$\mathbf{u}''-\left(-\mathbf{U}_{12}'\cdot\mathbf{U}_{12}^{-1}+\frac{\mathrm{i}k_0}{2}\mathbf{U}_{22}+\frac{\mathrm{i}k_0}{2}\mathbf{U}_{11}\right)\cdot\mathbf{u}'+\frac{k_0^2}{4}\mathbf{U}_{12}\cdot\mathbf{U}_{21}\cdot\mathbf{u}=\mathbf{0}$$

Appendix E Surface waves for homogeneous isotropic material

For an isotropic material that is homogeneous, the propagator is given by (2.14), see also [34, 35]. The pertinent parts of the propagator are

$$\begin{cases}\mathbf{P}_{12}(\boldsymbol{k}_t,d,0)=-\dfrac{\mathrm{i}}{\kappa}\sin\left(k_0d\kappa\right)\left\{\mu\mathbf{I}_2-\dfrac{\boldsymbol{k}_t\boldsymbol{k}_t}{k_0^2\epsilon}\right\}\\ \mathbf{P}_{22}(\boldsymbol{k}_t,d,0)=\mathbf{I}_2\cos\left(k_0d\kappa\right)\end{cases}$$

In the $\{\parallel,\perp\}$-coordinate representation, we get the TM-case and the TE-case, respectively. The result is

$$\begin{cases}P_{12}^{\mathrm{TM}}(k_t,d,0)=-\dfrac{\mathrm{i}\kappa}{\epsilon}\sin\left(k_0d\kappa\right)\\ P_{22}^{\mathrm{TM}}(k_t,d,0)=\cos\left(k_0d\kappa\right)\end{cases}\qquad\text{TM-case}\tag{E.1}$$

and

$$\begin{cases}P_{12}^{\mathrm{TE}}(k_t,d,0)=-\dfrac{\mathrm{i}\mu}{\kappa}\sin\left(k_0d\kappa\right)\\ P_{22}^{\mathrm{TE}}(k_t,d,0)=\cos\left(k_0d\kappa\right)\end{cases}\qquad\text{TE-case}\tag{E.2}$$

For a homogeneous, isotropic slab we thus have

$$\mathbf{W}^{-1}\cdot\mathbf{P}_{12}+\mathbf{P}_{22}=\mathbf{I}_2\cos(k_0d\kappa) - \frac{\mathrm{i}}{\kappa}\sin(k_0d\kappa)\left\{\frac{k_0}{k_z}\hat{\boldsymbol{e}}_\parallel\hat{\boldsymbol{e}}_\parallel+\frac{k_z}{k_0}\hat{\boldsymbol{e}}_\perp\hat{\boldsymbol{e}}_\perp\right\}\cdot\left\{\frac{\kappa}{\epsilon}\hat{\boldsymbol{e}}_\parallel\hat{\boldsymbol{e}}_\parallel+\mu\hat{\boldsymbol{e}}_\perp\hat{\boldsymbol{e}}_\perp\right\}$$

This expression can be simplified to

$$\cos(k_0d\kappa)-\frac{\mathrm{i}k_0\kappa}{k_z\epsilon}\sin(k_0d\kappa)=0,\quad\text{TM-case} \tag{E.3}$$

and

$$\cos(k_0d\kappa)-\frac{\mathrm{i}\mu k_z}{k_0\kappa}\sin(k_0d\kappa)=0,\quad\text{TE-case}$$

which are the transcendental equations that determine the k_t-value in a homogeneous, isotropic slab [10].

Appendix F Calculation of residues for a homogeneous substrate

The functions F^{TM} and G^{TM} that occur in the integral of the surface wave power are defined in (6.7). The residues of these functions can be computed explicitly for a homogeneous, isotropic substrate. As a step towards this, we compute the residue of the function

$$D(k_t)=k_zP_{22}^{\mathrm{TM}}(k_t,d,0)+k_0P_{12}^{\mathrm{TM}}(k_t,d,0)=k_z\cos(k_0d\kappa)-\frac{\mathrm{i}k_0\kappa}{\epsilon}\sin(k_0d\kappa)$$

The derivative w.r.t. k_t at the pole $k_t=k_{t\mathrm{sw}}$ is ($\kappa_{\mathrm{sw}}=\kappa_{k_t=k_{t\mathrm{sw}}}$, $k_{z\mathrm{sw}}=\sqrt{k_0^2-k_{t\mathrm{sw}}^2}$)

$$D'(k_{t\mathrm{sw}})=\sin k_0d\kappa_{\mathrm{sw}}\left(\frac{k_{t\mathrm{sw}}dk_{z\mathrm{sw}}}{k_0\kappa_{\mathrm{sw}}}-\frac{k_{t\mathrm{sw}}\cot k_0d\kappa_{\mathrm{sw}}}{k_{z\mathrm{sw}}}+\frac{\mathrm{i}k_{t\mathrm{sw}}}{\epsilon k_0\kappa_{\mathrm{sw}}}+\frac{\mathrm{i}k_{t\mathrm{sw}}d\cot k_0d\kappa_{\mathrm{sw}}}{\epsilon}\right)$$

or

$$D'(k_{t\mathrm{sw}})=\sin k_0d\kappa_{\mathrm{sw}}\left(\frac{k_{t\mathrm{sw}}dk_{z\mathrm{sw}}}{k_0\kappa_{\mathrm{sw}}}-\frac{\mathrm{i}k_0\kappa_{\mathrm{sw}}k_{t\mathrm{sw}}}{\epsilon k_{z\mathrm{sw}}^2}+\frac{\mathrm{i}k_{t\mathrm{sw}}}{\epsilon k_0\kappa_{\mathrm{sw}}}-\frac{k_0\kappa_{\mathrm{sw}}k_{t\mathrm{sw}}d}{\epsilon^2k_{z\mathrm{sw}}}\right)$$

where we have used the equation that determines the eigenvalue, *viz.*, see (E.3)

$$\cot k_0\kappa_{\mathrm{sw}}d=\frac{\mathrm{i}k_0\kappa_{\mathrm{sw}}}{\epsilon k_{z\mathrm{sw}}}$$

We simplify

$$D'(k_{t\mathrm{sw}})=\frac{k_{t\mathrm{sw}}}{\kappa_{\mathrm{sw}}}\sin k_0d\kappa_{\mathrm{sw}}\left(\frac{k_{z\mathrm{sw}}d}{k_0}-\frac{\mathrm{i}k_0\kappa_{\mathrm{sw}}^2}{\epsilon k_{z\mathrm{sw}}^2}+\frac{\mathrm{i}}{\epsilon k_0}-\frac{k_0d\kappa_{\mathrm{sw}}^2}{\epsilon^2k_{z\mathrm{sw}}}\right)$$

Finally, we get the residues of the functions F^{TM} and G^{TM} as

$$\begin{cases}\operatorname{Res}F^{\mathrm{TM}}(k_{t\mathrm{sw}},z)=\dfrac{k_zP_{12}^{\mathrm{TM}}(k_{t\mathrm{sw}},z,0)\eta_0J_S^{\mathrm{TM}}(k_{t\mathrm{sw}})}{D'(k_{t\mathrm{sw}})}\\[2ex]\operatorname{Res}G^{\mathrm{TM}}(k_{t\mathrm{sw}},z)=\dfrac{k_zP_{22}^{\mathrm{TM}}(k_{t\mathrm{sw}},z,0)\eta_0J_S^{\mathrm{TM}}(k_{t\mathrm{sw}})}{D'(k_{t\mathrm{sw}})}\end{cases}$$

References

[1] M. Abramowitz and I. A. Stegun, editors. *Handbook of Mathematical Functions*. Applied Mathematics Series No. 55. National Bureau of Standards, Washington D.C., 1970.

[2] N. G. Alexopoulos, P. B. Katehi, and D. Rutledge. Substrate optimization for integrated circuit antennas. *IEEE Trans. Microwave Theory Tech.*, **31**(7), 550–557, 1983.

[3] C. A. Balanis. *Antenna Theory*. John Wiley & Sons, New York, second edition, 1997.

[4] R. Bellman and G. N. Wing. *An Introduction to Invariant Imbedding*. John Wiley & Sons, New York, 1975.

[5] A. K. Bhattacharyya. Characteristics of space and surface waves in a multilayered structure. *IEEE Trans. Antennas Propagat.*, **38**(8), 1231–1238, 1990.

[6] L. M. Brekhovskikh. *Waves in layered media*. Academic Press, New York, second edition, 1980.

[7] W. C. Chew and J. A. Kong. Resonance of nonaxial symmetric modes in circular microstrip disc antenna. *J. Math. Phys.*, **21**(10), 2590–2598, 1980.

[8] W. C. Chew and J. A. Kong. Resonance of the axial-symmetric modes in microstrip disc resonators. *J. Math. Phys.*, **21**(3), 582–591, 1980.

[9] W. C. Chew. *Waves and fields in inhomogeneous media*. IEEE Press, Piscataway, NJ, 1995.

[10] R. E. Collin. *Field Theory of Guided Waves*. IEEE Press, New York, second edition, 1991.

[11] R. E. Collin. *Antennas and Radiowave Propagation*. McGraw-Hill, New York, 1985.

[12] R. E. Collin. *Foundations for Microwave Engineering*. McGraw-Hill, New York, second edition, 1992.

[13] N. K. Das and D. M. Pozar. A generalized spectral-domain Green's function for multilayer dielectric substrates with application to multilayer transmission lines. *IEEE Trans. Microwave Theory Tech.*, **35**(3), 326–335, March 1987.

[14] A. G. Derneryd. Analysis of the microstrip disk antenna element. *IEEE Trans. Antennas Propagat.*, **27**(5), 660–664, 1979.

[15] L. B. Felsen and N. Marcuvitz. *Radiation and scattering of waves*. Prentice-Hall, Inc., Englewood Cliffs, New Jersey, first edition, 1973.

[16] S. B. D. A. Fonseca and A. J. Giarola. Microstrip disk antennas, part I: Efficiency of space wave launching. *IEEE Trans. Antennas Propagat.*, **32**(6), 561–567, 1984.

[17] S. He, S. Ström, and V. H. Weston. *Time Domain Wave-splittings and Inverse Problems*. Oxford University Press, Oxford, 1998.

[18] P. Henrici. *Applied and Computational Complex Analysis*, volume 2. John Wiley & Sons, New York, 1977.

[19] H. How and C. Vittoria. Radiation modes in circular patch antennas. *IEEE Trans. Microwave Theory Tech.*, **42**(10), 1939–1944, 1994.

[20] D. M. Kokotoff, R. B. Waterhouse, and J. T. Aberle. On improving the surface wave efficiency of microstrip patches. In *Antennas and Propagation Society International Symposium, 1997. IEEE., 1997 Digest, Vol. 2*, pages 952–955, 1997.

[21] G. Kristensson, M. Åkerberg, and S. Poulsen. Scattering from a frequency selective surface supported by a bianisotropic substrate. Technical Report LUTEDX/(TEAT-7085)/1–28/(2000), Lund Institute of Technology, Department of Applied Electronics, Electromagnetic Theory, P.O. Box 118, S-211 00 Lund, Sweden, 2000.

[22] G. Kristensson. Radiation by an aperture antenna of arbitrary shape. Technical Report LUTEDX/(TEAT-7084)/1–32/(2000), Lund Institute of Technology, Department of Applied Electronics, Electromagnetic Theory, P.O. Box 118, S-211 00 Lund, Sweden, 2000.

[23] G. Kristensson, S. Poulsen, and S. Rikte. Propagators and scattering of electromagnetic waves in planar bianisotropic slabs — an application to frequency selective structures. Technical Report LUTEDX/(TEAT-7099)/1–32/(2001), Lund Institute of Technology, Department of Electroscience, P.O. Box 118, S-211 00 Lund, Sweden, 2001.

[24] Y. T. Lo, D. Solomon, and W. F. Richards. Theory and experiment on microstrip antennas. *IEEE Trans. Antennas Propagat.*, **27**(2), 137–145, 1979.

[25] S. A. Long, L. C. Shen, and P. B. Morel. Theory of the circular-disc printed-circuit antenna. *Proc. IEE*, **125**(10), 925–928, 1978.

[26] V. Losada, R. R. Boix, and M. Horno. Resonant modes of circular microstrip patches in multilayered substrates. *IEEE Trans. Microwave Theory Tech.*, **47**(4), 488–498, 1999.

[27] V. Losada, R. R. Boix, and M. Horno. Full-wave analysis of circular microstrip resonators in multilayered media containing uniaxial anisotropic dielectrics, magnetized ferrites, and chiral materials. *IEEE Trans. Microwave Theory Tech.*, **48**(6), 1057–1064, 2000.

[28] V. Losada, R. R. Boix, and M. Horno. Resonant modes of circular microstrip patches over ground planes with circular apertures in multilayered substrates containing anisotropic and ferrite materials. *IEEE Trans. Microwave Theory Tech.*, **48**(10), 1756–1762, 2000.

[29] K. M. Luk, W. Y. Tam, and C. L. Yip. Analysis of circular microstrip antennas with superstrate. *IEE Proceedings*, **136**(3), 261–262, 1989.

[30] M. Norgren. *Wave-Splitting Approaches to Direct and Inverse Frequency-Domain Scattering of Electromagnetic Waves from Stratified Bianisotropic Materials*. PhD thesis, Royal Institute of Technology, Stockholm, Sweden, 1996.

[31] D. M. Pozar. Rigorous closed-form expressions for the surface wave loss of printed antennas. *Electronics Letters*, **26**(13), 954–956, 1990.

[32] D. M. Pozar. *Microwave Engineering*. John Wiley & Sons, New York, 1998.

[33] S. Rikte, M. Andersson, and G. Kristensson. Homogenization of woven materials. *Archiv für Elektronik und Übertragungstechnik (AEÜ)*, **53**(5), 261–271, 1999.

[34] S. Rikte, G. Kristensson, and M. Andersson. Propagation in bianisotropic media—reflection and transmission. Technical Report LUTEDX/(TEAT-7067)/1–31/(1998), Lund Institute of Technology, Department of Electromagnetic Theory, P.O. Box 118, S-211 00 Lund, Sweden, 1998.

[35] S. Rikte, G. Kristensson, and M. Andersson. Propagation in bianisotropic media—reflection and transmission. *IEE Proc.-H Microwaves, Antennas and Propagation*, **148**(1), 29–36, 2001.

[36] L. C. Shen, S. A. Long, M. R. Allerding, and M. D. Walton. Resonant frequency of a circular disc, printed-circuit antenna. *IEEE Trans. Antennas Propagat.*, **25**(4), 595–596, 1977.

[37] X.-H. Shen, P. Delmotte, and G. A. E. Vandenbosch. Effect of superstrate on radiated field of probe fed microstrip patch antenna. *IEE Proc. Microwaves, Antennas and Propagation*, **148**(3), 141–146, 2001.

[38] X.-H. Shen, A. E. Vandenbosch, and A. R. V. de Capelle. Study of gain enhancement method for microstrip antennas using moment method. *IEEE Trans. Antennas Propagat.*, **43**(3), 227–231, 1995.

[39] L. Vegni, F. Bilotti, and A. Toscano. Microstrip disk antennas with inhomogeneous artificial dielectrics. *J. Electro. Waves Applic.*, **14**(9), 1203–1227, 2000.

[40] L. Vegni and A. Toscano. Full-wave analysis of planar stratified media with inhomogeneous layers. *IEEE Trans. Antennas Propagat.*, **48**(4), 631–633, 2000.

[41] J. R. Wait. *Electromagnetic Waves in Stratified Media*. Pergamon, New York, second edition, 1970.

[42] J. J. H. Wang. *Generalized Moment Methods in Electromagnetics: Formulation and Computer Solution of Integral Equations*. John Wiley & Sons, New York, 1991.

[43] W. Wasow. *Asymptotic Expansion for Ordinary Differential Equations*. Dover Publications, New York, 1965.

[44] J. Watkins. Circular resonant structures in microstrip. *Electronics Letters*, **5**(21), 524–525, 1969.